HHS Public Access

Author manuscript

Cell Rep. Author manuscript; available in PMC 2024 March 30.

Published in final edited form as:

Cell Rep. 2024 March 26; 43(3): 113823. doi:10.1016/j.celrep.2024.113823.

Kin17 regulates proper cortical localization of Miranda in *Drosophila* neuroblasts by regulating Flfl expression

Marisa Connell[1,2], **Yonggang Xie**[1,3], **Xiaobing Deng**[1], **Rui Chen**[1,3], **Sijun Zhu**[1,4,*]

[1]Department of Neuroscience and Physiology, State University of New York Upstate Medical University, Syracuse, NY 13210, USA

[2]Current Address: Department of Biological Sciences, Louisiana State University Shreveport, Shreveport, LA 71115, USA

[3]Current Address: GeneScript USA, Inc, Piscataway, NJ 08854, USA

[4]Lead contact

Abstract

During asymmetric division of *Drosophila* larval neuroblasts, the fate determinant Prospero (Pros) and its adaptor Miranda (Mira) are segregated to the basal cortex through aPKC phosphorylation of Mira and displacement from the apical cortex, but Mira localization after aPKC phosphorylation is not well understood. We identify Kin17, a DNA replication and repair protein, as a regulator of Mira localization during asymmetric cell division. Loss of Kin17 leads to aberrant localization of Mira and Pros to the centrosome, cytoplasm, and nucleus. We provide evidence to show that the mislocalization of Mira and Pros is likely due to reduced expression of Falafel (Flfl), a component of protein phosphatase 4 (PP4), and defects in dephosphorylation of Serine-96 of Mira. Our work reveals that Mira is likely dephosphorylated by PP4 at the centrosome to ensure proper basal localization of Mira after aPKC phosphorylation and that Kin17 regulates PP4 activity by regulating Flfl expression.

Graphical Abstract

[*]Correspondence to: Sijun Zhu, PhD, Upstate Medical University, 4611 Institute for Human Performance, 505 Irving Ave, Syracuse, NY 13210, zhus@upstate.edu.

Author Contributions

Conceptualization, M.C., Y.X., and S.Z.; Methodology; Investigation, M.C., Y.X., X.D., R.C., and S.Z.; Writing- Original Draft, M.C. and S.Z, Writing- Review & Editing- M.C. and S.Z., Supervision, M.C., and S.Z.; Funding, S.Z.

Declaration of Interests

The authors declare no competing interests.

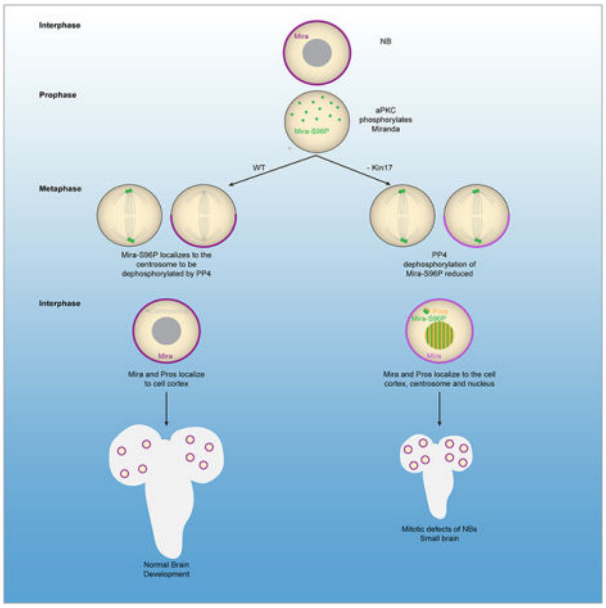

Summary:

Connell et al. identify a regulator of Miranda localization, Kin17, which promotes the proper localization of Mira by regulating the expression of PP4 component Falafel. They further show that proper segregation of the cell fate determinant Mira likely requires PP4-mediated dephosphorylation of Serine-96 of Mira at the centrosome and subsequent dissociation of Mira from the centrosome/spindle in *Drosophila* neuroblasts, a critical step that has been overlooked previously.

Keywords

Drosophila; neuroblast; Kin17; Miranda; Prospero; Falafel; protein phosphatase 4; splicing

Introduction

The generation of diverse cell types from a single population of stem cells is essential for proper development. In the brain, neural stem cells (NSCs) divide to produce neurons and glia. Asymmetric cell division allows for the generation of cells of different fates from one parental cell by producing daughters of different protein content, fate, niche, and/or size. This process must be tightly regulated to ensure the proper balance of stem and differentiating cells, and defects in this process can lead to overproliferation or premature differentiation of the stem cell population, both of which can have detrimental effects on the organism, such as cancer or developmental disorders.[1]

Drosophila NSCs, termed neuroblasts (NBs), provide a useful model for the study of asymmetric cell division as many of the key components are conserved in mammalian systems.[2] In developing *Drosophila* brains, most NBs (type I NBs) divide asymmetrically to generate a self-renewing NB and a differentiating ganglion mother cell (GMC).[2] GMCs divide a single time to produce neurons and glia. The identity of the GMC is established

by the specific segregation of the fate determinants, Prospero (Pros)[3,4], Numb4, and Brain tumor (Brat)[5–7] to the GMC during mitosis. In order to deliver these factors to the GMC, neuroblasts establish a cell polarity axis during mitosis through the recruitment of the Par protein complex to the apical pole of the cell.[8,9] This apical complex establishes cell polarity by excluding the localization of the fate determinants from the apical pole, leading to basal localization of these factors.

One of the primary factors that must be excluded from the apical pole is the adaptor protein, Miranda (Mira), which localizes *pros* mRNA[10], Pros[11,12], Staufen[13], and Brat[6] to the basal pole and ensures their proper segregation to the GMC. Prior to the onset of mitosis, Mira localizes to the entire cell cortex through an interaction between its Basic and Hydrophobic (BH) motif and the cell membrane[14]. At the onset of mitosis, Inscuteable and Bazooka (Baz, also known as Par-3) are recruited to the apical cortex, where Cdc42 acts downstream of Baz to recruit the Par-6/aPKC (atypical Protein Kinase C) complex to the cortex through a direct interaction between the CRIB domain of Par-6 and Cdc42.[15–19] This interaction between Par-6 and Cdc42 relieves the Par-6-mediated suppression of the serine/threonine kinase activity of aPKC[19], and subsequently, aPKC phosphorylates Mira within the BH motif breaking the interaction between Mira and the apical cell cortex, leading to basal localization.[14,20] Although aPKC phosphorylates multiple residues, a phosphomimetic mutation of S96, Mira^{S96D}, is displaced from the cortex even in the absence of aPKC, indicating that phosphorylation of S96 is sufficient for displacement from the cortex.[20] This raises the question of how Mira localizes to the basal cortex after aPKC phosphorylation. A previous study reports that depletion of Falafel (Flfl), the targeting subunit of Protein Phosphatase 4 (PP4), leads to a reduction in Mira localization to the basal domain[21], implying that Mira needs to be dephosphorylated before interacting with the basal domain. However, while Flfl has been shown to physically interact with Mira[21], PP4 has only been shown to be required for the dephosphorylation of threonine-591, which is required for cortical localization of Mira prior to its phosphorylation by aPKC.[22] Therefore, although how Mira is phosphorylated by aPKC and displaced from the apical cortex has been well studied, the exact mechanism of how Mira localizes to the basal cortex after aPKC phosphorylation is unclear.

Mira has also been shown to localize to the centrosome of wild-type NBs during prophase[23] and to the mitotic spindle in syncytial embryos and various mutants, including Mira^{S96D}.[18,19,23–25] The mutants that lead to accumulation of Mira to the centrosome and mitotic spindle also lead to defects in basal localization, suggesting that the localization of Mira to the centrosome in prophase and its clearance may be an essential step in localization to the basal domain downstream of aPKC phosphorylation.

Kin17 is known as a DNA- and RNA-binding protein that is essential for DNA replication and DNA damage repair.[26–29] Kin17 is upregulated in cervical[30], breast[31–33], colorectal[34], ovarian[35], and lung cancers[36], where it is associated with proliferation and invasion. Here, we identify Kin17 as a factor regulating the localization of Mira during asymmetric cell division in *Drosophila* larval NBs. We demonstrate that Kin17 promotes the proper localization of Mira in part by regulating the expression of the PP4 component Flfl. We further show that PP4 likely dephosphorylates Mira at S96 at the centrosome to ensure

dissociation of Mira and Pros from the centrosome/spindle and proper cortical localization. Therefore, our work reveals a mechanism that ensures proper localization of Mira during the asymmetric division of NBs.

Results

Kin17 knockdown leads to reduced brain size and a reduced mitotic index in NBs

We identified Kin17 in a screen for factors that affect *Drosophila* brain development. Kin17 knockdown using the pan-neuroblast (NB) driver, *insc-Gal4*, led to reduced brain size (Figs. 1A,B). This decrease in brain size was not due to a reduction in the number of type I NBs in the central brain (Figs. 1C,D). However, we observed a significant decrease in the mitotic index of *Kin17 RNAi* NBs (Figs. 1E,F) and a corresponding reduction in GMCs (Pros+, Elav-) and newly born neurons ($Pros^{+}$, $Elav^{+}$) (Fig. 1G,H). These phenotypes were rescued by expressing Kin17, ruling out off-target effects of the RNAi (Figs. 1A,B,E–H). These results indicate that Kin17 is required for normal brain development and mitosis in NBs.

Kin17 knockdown leads to aberrant nuclear and centrosomal accumulation of Pros

Nuclear Pros promotes cell cycle exit of GMCs[37] and quiescence or premature differentiation in NBs.[38] Therefore, we examined if the reduction in the mitotic index of *Kin17 RNAi* NBs was caused by Pros localization to the nucleus. We observed that 37.5± 15.0% of *Kin17 RNAi* NBs had nuclear Pros (Figs. 1I,J), which was never observed in control NBs. To determine if the aberrant nuclear Pros is responsible for the Kin17 knockdown phenotypes, we examined if reducing Pros levels would alleviate the Kin17 phenotypes. Kin17 knockdown in $pros^{17/+}$ NBs leads to a signification reduction in nuclear Pros localization (Figs. 1K,L), the mitotic index was partially rescued to 20.2 ± 2.8% compared to 34.3% in control and 13.4% in *Kin17 RNAi* (Figs. 1M,N), and the reduction in Pros+ neurons, GMCs, and brain volume was also partially rescued (Fig. 1O–Q), suggesting that the Kin17 phenotypes are due to aberrant nuclear localization of Pros.

In addition to the nuclear localization, we also observed significantly increased centrosomal localization of Pros at interphase and metaphase (particularly at the apical centrosome) in *Kin17 RNAi ; pros*$^{17/+}$ NBs (Figs 2A,B) as indicated by its colocalization with the centrosomal protein, Pericentrin-like protein (Plp).[39] In control NBs, centrosomal Pros appeared to be cell cycle-dependent, with a peak occurring in prophase (Figs.2A,B). However, Pros basal crescents were observed at similar rates in control and Kin17 RNAi; $pros^{17/+}$ NBs at metaphase (Fig. S1A,B). Therefore, Kin17 is required to prevent aberrant localization of Pros to the nucleus and centrosome.

Kin17 is required for proper Mira localization

As Mira is the adaptor protein of Pros[11], we asked if Mira localization was altered in *Kin17 RNAi* NBs. In control NBs, Mira localized to the cortex during interphase as previously described (Figs. 2C). During prophase, Mira showed increased localization to the apical centrosome, which decreases through the rest of cell cycle until it returns to interphase levels in telophase (Figs. 2C,D).[23] Similar to Pros, we found Mira also aberrantly localized to the centrosome in Kin17 RNAi NBs in interphase (Fig. 2C,D). Since Kin17 RNAi NBs

have a low mitotic index and, we performed Kin17 RNAi in the *pros*$^{17/+}$ background to systematically quantify Mira localization at different stages of the cell cycle. Pros is not required for proper Mira localization[12] and Mira localization in *pros*$^{17/+}$ NBs was similar to that in the control throughout the cell cycle (Fig. 2C,D). In *Kin17 RNAi; pros*$^{17/+}$ NBs, there was a significant increase in Mira centrosomal localization in interphase and telophase and at the basal centrosome in prophase and metaphase (Figs. 2C,D). Besides the centrosomal localization, about 25% of Kin17 knockdown NBs also exhibited Mira localization to the mitotic spindle at anaphase/telophase, which was only observed in 3–6% of control or *pros*$^{17/+}$ NBs (Fig. 2C). Furthermore, we found that Mira accumulation at the centrosome correlated with defects in cortical localization, with 24.8% and 9.1% of *Kin17 RNAi; pros*$^{17/+}$ NBs having cytoplasmic Mira at interphase and metaphase, respectively, as well as reduced basal cortical localization in 20–30% of prophase and metaphase NBs (Figs. 2E,F). Mira centrosomal localization was significantly correlated with Pros centrosomal localization in interphase *Kin17 RNAi* NBs. Among NBs with centrosomal localization of Mira, about 80% of them exhibited a centrosomal Pros to cytoplasmic Pros ratio of greater than 1.5 (Figs. 2G,H); whereas among the NBs with centrosomal localization of Pros, 93% of them also showed a centrosomal Mira to cytoplasmic Mira ratio of greater than 1.5 (Fig. S1C). In addition, we observed nuclear localization of Mira that was also correlated with Pros nuclear localization in Kin17 knockdown NBs at the interphase (Figs. S1D,E). Taken together, our data suggest that Kin17 regulates Mira localization in a cell cycle-dependent manner and that aberrant centrosomal and nuclear Mira localization correlates with of Pros localization to the centrosome and nucleus. This regulation appears to be specific as we did not observe mislocalization of the basal component Numb in Kin17 knockdown NBs (Figs. S2A,B).

Kin17 RNAi can potentially lead to defects in asymmetric cell division of NBs

Although we observed defects in Mira localization at metaphase during Kin17 knockdown, we rarely saw defects in basal cortical localization at telophase. The lack of basal cortical localization defects of Mira at the telophase could be due to correction of the Mira localization defects in a process known as “telophase rescue”[40] and may account for the fact we did not observe changes in the number of type I NBs during Kin17 RNAi. Telophase rescue involves Eiger and Traf4.[40,41] In order to examine if Kin17 RNAi could affect asymmetric division of NBs, we thus inhibited telophase rescue by Eiger RNAi. Eiger RNAi alone did not change the basal cortical localization of Mira or the number of type I NBs (Figs. 2I,J, S2C,D). Interestingly, Kin17 and Eiger double knockdown led to a loss of basal cortical localization of Mira in about 80% of telophase NBs and about a 5% increase in the number of type I NBs (Figs. 2I,J, S2C,D), indicating that Kin17 knockdown can lead to defects in asymmetric cell division when there is no telophase rescue. The increase in the number of type I NBs was small probably because most Kin17 RNAi NBs were not actively dividing due to the aberrant nuclear localization of Pros.

Phosphorylation at Serine-96 leads to centrosomal localization of Mira

As localization of Mira to the centrosome in wild-type NBs occurs in prophase when aPKC is recruited to phosphorylate Mira, we hypothesized that phosphorylation of Mira leads to its centrosomal localization and that defects in dephosphorylation are leading to accumulation

of Mira to the centrosome and cortical localization defects in Kin17 RNAi NBs. Serine-96 (S96) is phosphorylated by aPKC and this phosphorylation is required and sufficient for the displacement of Mira from the cell cortex.[14,20,24] However, it is currently unknown if Mira is dephosphorylated prior to localization at the basal cortex. To directly assess if phosphorylation of S96 regulates the localization of Mira to the centrosome, we utilized phosphomutant alleles of *mira*. We observed that $Mira^{WT}$ localizes similarly to endogenous Mira, except that in anaphase/telophase, $Mira^{WT}$ was enriched at the centrosome and/or mitotic spindle in about 20% of NBs (Figs. 3A,B, S3A, compared to Figs. 2C,D,F). For phosphomimetic $Mira^{S96D}$, we observed an increase in cytoplasmic localization at interphase and prophase (Fig. S3A), and increased centrosomal localization through the entire cell cycle (Figs. 3A, B). In contrast, the phosphodead $Mira^{S96A}$ primarily localized to the cell cortex and rarely to the centrosome at all stages (Figs 3A,B, S3A). The lack of centrosomal localization of $Mira^{S96A}$ is unlikely due to sequestration at the cortex as $Mira^{S96A}$ could not localize to the mitotic spindle either as $Mira^{WT}$ and $Mira^{S96D}$ did in syncytial embryos, which lack cell membranes (Fig. 3C). Therefore, the mislocalization of Mira to the centrosome observed in Kin17 knockdown NBs is likely due to phosphorylation of Mira on S96.

Next, we asked if aberrant phosphorylation of Mira is responsible for the localization of Pros to the nucleus and centrosome observed in Kin17 knockdown NBs. We examined Pros localization in embryonic NBs homozygous mutant for the phosphomutant *mira* alleles. We observed that Pros localized to the nucleus in 20 ± 8.7% of $mira^{S96D}$ NBs compared to 0% and 5.6 ± 7.9% for $mira^{WT}$ and $mira^{S96A}$ NBs, respectively, at the interphase (Figs. 3D,E). Accordingly, we observed a significant increase in Pros localization to the centrosome in interphase $mira^{S96D}$ NBs compared to $mira^{WT}$ and $mira^{S96A}$ NBs (Figs. 3D,F,G). These results suggest that nuclear and centrosomal Pros localization observed in *Kin17 RNAi* NBs could be due to phosphorylation of S96 of Mira.

PP4 dephosphorylates Mira at Serine-96

Aberrant Mira phosphorylation could be due to an increase in aPKC activity or a decrease in phosphatase activity. We observed that localization of apical Bazooka and aPKC were not altered in Kin17 knockdown during metaphase (Figs. S4A,B), but we observed aPKC localization to the cell cortex was reduced relative to the cytoplasm when compared to Kin17 rescue, suggesting that there is a reduction in aPKC levels (Figs. S4C). Together, this suggests that Kin17 may function through a phosphatase.

Falafel (Flfl), the targeting subunit of Protein Phosphatase 4 (PP4), is required for basal Mira localization and interacts with Mira, and PP4 is required for dephosphorylation of Mira at T591[21,22.] However, it has not been shown if PP4 is required for dephosphorylation at S96. To test if PP4 dephosphorylates Mira at S96, we first examined the role of PP4 in Mira centrosomal localization. We found that knockdown of Flfl or the catalytic subunit of PP4, PP4–19c, led to increased Mira localization to the centrosome throughout the cell cycle (Figs. 4A,B). Furthermore, $flfl^{n42}$ mutants exhibited nuclear Pros localization in 52.5% of NBs and a significant reduction in the mitotic index (Figs. S4D–G). However, we did not observe increased centrosomal localization of $Mira^{T591D}$ in NBs compared to $Mira^{WT}$

or MiraT591A (Figs. S4H,I). These phenotypes suggest that decreased PP4 activity but not defects in dephosphorylation at T591 could account for the aberrant centrosomal localization of Mira in Kin17 knockdown NBs.

To further test if PP4 can dephosphorylate Mira at S96, we utilized an *in vitro* malachite green-based phosphatase assay. We immunoprecipitated the PP4 complex from *Drosophila* S2 cells (Fig. 4C, left) and incubated this with a synthetic phospho-peptide corresponding to the region surrounding S96 [92-FRTP(pSer)LPQR-100]. We found that incubating PP4 immunoprecipitates with the Mira pS96 peptide led to a 3.6-fold increase in dephosphorylation compared to IgG immunoprecipitates (Fig. 4C, right). These data together with the similar centrosomal localization of Mira observed in Flfl/PP4-19c knockdown NBs and Kin17 knockdown/Mira^{S96D} mutant NBs strongly suggest that PP4 can dephosphorylates Mira at S96 and reduced PP4 activity and subsequent defects in Mira dephosphorylation at S96 is likely responsible for the aberrant Mira localization in Kin17 knockdown NBs.

The PP4 complex localizes to centrosomes and the mitotic spindle

We next wanted to identify the localization of the PP4 complex in NBs. In NBs, Flfl localizes to the nucleus during interphase.[21] However, in *Drosophila* D.mel-2 cells, Flfl localizes to the kinetochores[42] and PP4 is centrosomal in *Drosophila embryos*.[43,44] To visualize the localization of Flfl in NBs, we utilized *UAS-RFP-Flfl*[21], which localized to the nucleus in interphase and was enriched at the centrosome and mitotic spindle in 67.3% of mitotic NBs (Fig. 4D). Additionally, PP4-19c was significantly enriched at the apical centrosome during mitosis compared to interphase and this enrichment at the apical centrosome diminished after PP4-19c knockdown (Figs. 4E,F). The localization of Flfl and PP4 supports a model that Mira is dephosphorylated by PP4 at the centrosome.

To investigate if Flfl functions at the centrosome to dephosphorylate Mira, we targeted Flfl specifically to the centrosome using the PACT domain of Plp.[45,46] We quantified Mira localization in prophase NBs expressing V5-Flfl-PACT and found that targeting Flfl to the centrosome lead to a significant reduction in Mira localization to the centrosome during prophase (Figs. 4G,H). A similar reduction was not observed when we overexpressed V5-PACT (Figs. 4G,H), indicating that targeting Flfl to the centrosome via the PACT domain may account for this difference and supporting the idea that Flfl/PP4 dephosphorylates Mira at the centrosome.

The centrosome is required for dephosphorylation and basal localization of Mira

The localization of the PP4 complex to the centrosome and the reduction in Mira centrosomal localization when Flfl-PACT is over-expressed suggests that dephosphorylation of Mira occurs at the centrosome. However, Mira could accumulate to the centrosome because of defects in dephosphorylation rather than as part of the dephosphorylation mechanism. To test that Mira dephosphorylation occurs at the centrosome, we knocked down *Sas-4*. Sas-4 is required for centriole replication and centrosomes are completely lost in Sas-4 RNAi NBs at late larval stages, although NBs assemble mitotic spindles and undergo mitosis.[47] We hypothesized that if dephosphorylation of Mira did not require the

centrosome, Mira would still localize to the basal domain during mitosis. We confirmed that Flfl levels and aPKC localization were not altered in *Sas-4 RNAi* NBs (Figs. 5A–D). Knockdown of Sas-4 led to an increase in cytoplasmic Mira localization in interphase, prophase, and metaphase (Figs. 5E,F), demonstrating that the centrosome is essential for proper cortical localization of Mira. We then combined *Sas-4 RNAi* with the Mira S96 phosphomutants and found that *Sas-4 RNAi* with the $mira^{S96D}$ allele led to a more severe phenotype in metaphase and telophase than $mira^{S96D}$ alone or *Sas-4 RNAi* combined with $mira^{WT}$ (Figs. 5G,H). In contrast, MiraS96A remained consistently cortical in *Sas-4 RNAi* NBs, indicating that increased cytoplasmic localization of Mira in *Sas-4 RNAi* NBs is due to enhanced phosphorylation at S96. In both experiments, we observed that endogenous Mira and $Mira^{WT}$ showed increased cytoplasmic localization during interphase (prior to aPKC phosphorylation). This is likely because Mira could not be dephosphorylated properly in the previous rounds of mitosis due to the lack of the centrosome. Subsequently, the phosphorylated Mira could not be was fully segregated to the daughter GMC and remained in the cytoplasm of newly generated NBs during interphase. Further, the phosphorylated Mira may also bring the newly synthesized unphosphorylated Mira to the cytoplasm by forming dimmers. Together, these data indicate that the centrosome is required for proper cortical localization of Mira and that defects in cortical localization of Mira in NBs lacking the centrosome is likely due to defects in S96 dephosphorylation.

We then tested if Mira phosphorylation levels at S96 was increased in *Sas-4 RNAi* brains, utilizing an antibody specific to phosphorylated Phospho-(Ser) 14-3-3 binding motif which has the same sequence as the region surrounding S96 of Mira and was confirmed to specifically recognize Mira phosphorylated at S96 (Fig. 5I). We found that there was an increase in pS96 Mira relative to total Mira in *Sas-4 RNAi* brains compared to control brains (Fig. 5J,K), indicating that *Sas-4 RNAi* leads to an increase in Mira phosphorylated at S96. Taken together, these data indicate that dephosphorylation of Mira by PP4 likely occurs at the centrosome and this is required for proper basal cortical localization of Mira.

Kin17 regulates cellular levels of Flfl

We then investigated if Kin17 regulates PP4 activity by examining the expression of Flfl and PP4-19c. We found that Kin17 RNAi led to a reduction in Flfl levels to about half that observed in control interphase NBs (Figs. 6A,B). Additionally, we found a change in PP4-19c localization from nuclear to cytoplasmic at interphase (Figs. 6C). In *Dictyostelium*, SMEK, a Flfl homolog, is required for PP4C to localize to the nucleus.[48] Therefore, the cytoplasmic localization of PP4-19c in *Kin17 RNAi* NBs could be due to the reduction in Flfl expression. Indeed, PP4-19c became cytoplasmic in $flfl^{n42}$ mutant NBs (Figs. 6C,D).

The minor spliceosome component U6atac regulates Mira localization and Flfl expression

As previous experiments suggest that Kin17 may be involved in splicing[49–52] and *Kin17 RNAi* led to a reduction in the levels of Flfl, we hypothesized that Kin17 may regulate the splicing of *the flfl* transcript. To test this hypothesis, we examined how loss of the major or minor spliceosomes would affect Mira localization. Knockdown of the major spliceosome component, U2A, did not lead to Mira mislocalization (Figs. 7A,B). However, there was a significant increase in Mira localization to the centrosome in interphase and telophase and

to the basal centrosome in prophase and metaphase in NBs homozygous mutant for *u6atac* (*u6atac*^{k01105}), a minor spliceosome component (Figs. 7A,B). Furthermore, we observed Mira cortical localization defects in *u6atac*^{k01105} mutants (Figs. 7C,D). Consistent with the mislocalization of Mira, Pros localized to the nucleus in 45 ± 19.7% of *u6atac*^{k01105} NBs (Figs. 7E,F). Consequently, the mitotic index of *u6atac*^{k01105} mutant NBs was reduced to 14.4 ± 3.1% from 26.3 ± 5.9% in the control (Figs. 7G,H). Additionally, loss of U6atac led to a reduction in Flfl levels by 56% and localization of PP4-19c to the cytoplasm (Figs. 7I–K). These phenotypes are similar to those observed in Kin17 RNAi NBs, suggesting that Kin17 could function in splicing of the *flfl* pre-mRNA. Consistent with a role in splicing, Kin17-HA localized to the nucleus when expressed in NBs (Fig. 7L).

Kin17 interacts with the flfl *mRNA*s and knockdown of Kin17 leads to a reduction in flfl mRNAs

To assess if Kin17 and U6atac are involved in regulating splicing of *flfl* pre-mRNAs, we performed quantitative real-time PCR using primers to the mRNA of *flfl*. We found that in both *Kin17 RNAi* and *u6atac*^{k01105} larval brains, there was a reduction in the spliced form of the *flfl mRNA* relative to control and eEF1a1 (Fig. 7M). Furthermore, immunoprecipitation of Kin17-HA from embryos showed that Kin17 interacts with the *flfl* mRNA (Fig. 7N). Although we were not able to immunoprecipitate *flfl* pre-mRNAs likely due to low abundance, the reduction in *flfl* mRNAs in Kin17 RNAi and *u6atac*^{k01105} mutant brains and binding of Kin17 to *flfl* mRNAs support the hypothesis that Kin17 is required for splicing of the *flfl* mRNA. However, Kin17 may not just specifically bind to *flfl* mRNAs. We observed that *aPKC* mRNAs and *pr*os mRNAs were also immunoprecipitated by Kin17 (Fig. 7O). Given that aPKC expression was also reduced in Kin17 RNAi NBs, it is possible that Kin17 may be involved in pre-mRNA splicing of other genes such as *aPKC*.

Discussion

We have identified Kin17 as essential for the proper localization of Mira in *Drosophila* NBs. The localization of Mira during asymmetric division is essential to the proper segregation of the fate determinants to the daughter cell and the regulation of its phosphorylation state via an interplay between kinases and phosphatases is essential to this localization. We demonstrate that PP4 is required for the dephosphorylation of Mira at S96 at the centrosome beginning in prophase and completing dephosphorylation by the end of mitosis. Dephosphorylation of Mira at the centrosome is essential for proper localization of Mira to the basal domain and prevents accumulation of Mira at the centrosome and in the cytoplasm. Knockdown of Kin17 leads to reduction in Flfl expression and PP4 activity, consequently, Mira cannot be fully dephosphorylated at S96 and accumulates in the cytoplasm and the centrosome instead of binding to the basal cortex, which leads to Pros being translocated to the nucleus. Further, similar mislocalization of Mira/Pros and reduction in *flfl* mRNAs observed in *u6atac* mutant and Kin17 knockdown NBs and binding of Kin17 to *flfl* mRNAs suggest that Kin17 is likely involved in *flfl* splicing.

Kin17 has not been well-studied in *Drosophila*. In mammals, it is essential for DNA repair and replication. Kin17 has been shown to interact with the spliceosome[49,51,52] and has

very recently been identified as a splicing factor in *C. elegans*, where Kin17 is required to maintain the 5' splice site identity during spliceosome assembly.[50] In this system, mutations in Kin17 led to changes in alternative 5' splice site usage.[50] Kin17 may play a similar role in humans, as mass spectrometry has identified it to primarily interact with the spliceosome in B stage, which is the first formation of the entire spliceosome.[49] Here we show that Kin17 binds to *flfl* mRNAs and knockdown of Kin17 leads to reduction in *flfl* mRNAs, and that mutants for the minor spliceosome component *u6atac* phenocopy Kin17 knockdown, supporting that in *Drosophila* Kin17 functions to regulate splicing of transcripts. In the mass spectrometry analysis, Kin17 was only found in complexes isolated from both HeLa and *Drosophila* Kc cells using *fushi tarazu* as bait but not *zeste*[51], suggesting that Kin17 likely regulates splicing of specific transcripts rather than acting as a general splicing factor. However, Kin17 may not just regulates the splicing of *flfl* pre-mRNAs in the NBs as Kin17 also binds to *aPKC* and *pros* mRNAs and Kin17 knockdown also leads to reduction in aPKC expression. It is possible that Kin17 may also regulate splicing of other transcripts such as aPKC transcripts. Our findings that Kin17 is potentially involved in regulating splicing of particular transcripts could be helpful for investigating underlying mechanisms of pathogenesis of various cancers associated with increased Kin17 expression.[30,31,34,36,53]

Mira localization to the mitotic spindle/centrosome has been observed in the syncytial embryo[23], and interactions between Mira and the microtubules have also been observed in the anterior pole of oocytes.[54] Mutants in polarity proteins can lead to localization of Mira to the centrosome and mitotic spindle in NBs, raising the question of why Mira does not localize to the mitotic spindle in NBs, and whether localization to the mitotic spindle during mitosis leads to consequences for asymmetric cell division. Our work provides evidence that localization to the centrosome and potentially the mitotic spindle (based on the S96 alleles) does occur in wild-type NBs but it is likely transient and appears to be cell-cycle dependent. Our work also reveals that localization of Mira to the centrosome/spindle depends on the phosphorylation status of Mira at S96 and that localization of Mira to the centrosome is essential for dephosphorylation of S96 and cortical localization as *Sas-4 RNAi* leads to defects in cortical localization and an increase in the levels of phosphorylated Mira. Although PP4 has been implicated in dephosphorylation of Mira at T59122, our work identifies S96 as a dephosphorylation site of PP4 and shows that T591 phosphorylation does not contribute to the observed phenotype. In fact, we observed a slight decrease in T591D centrosomal localization. This may be due to the fact that T591 dephosphorylation is required prior to aPKC phosphorylation of Mira to ensure proper localization.[22] Thus, Mira removal from the centrosome is specific to dephosphorylating S96. Our finding of dephosphorylation of S96 by PP4 at the centrosome answers several outstanding questions regarding Mira localization after aPKC phosphorylation, including if PP4 dephosphorylates Mira, the function of centrosomal localization of Mira, and if dephosphorylation of S96 occurs prior to localization of Mira to the basal domain.

Interestingly, we observed an increase of Mira localization to the centrosome in *PP4* and *Flfl RNAi* NBs with a minimal increase in cytoplasmic Mira. This suggests that centrosomal/spindle localization of Mira may be more sensitive to changes in the levels of PP4 activity. The phosphorylated Mira may preferentially localize to the centrosome/spindle and bring its cargo protein Pros to the centrosome as well as indicated by the colocalization of Pros

and Mira to the centrosome in *Kin17 RNAi* NBs. Additionally, in Kin17 RNAi NBs, we observed defects in Mira cortical localization in interphase, which is likely related to the localization of Pros to the nucleus. *mira* null mutants exhibit nuclear Pros localization[24], suggesting that Pros must be tethered to something to prevent nuclear localization and that defects in S96 dephosphorylation cause tethering to the cortex to be impaired so Mira/Pros then localizes to the centrosome and nucleus. It is tempting to speculate that when the amount of phosphorylated Mira exceeds the binding capacity of the centrosome/spindle, it may "overflow" to the cytoplasm, leading to untethered Pros being transported into the nucleus.

In summary, our studies identify a factor, Kin17, that regulates the proper localization of Mira during asymmetric cell division potentially through regulation of the splicing of *flfl* transcripts and provides evidence to demonstrate that dephosphorylation of Mira at S96 by PP4 at the centrosome is essential for proper localization of Mira in NBs during asymmetric cell division.

Limitations of the Study

There are several limitations to the study that prevent making further conclusions. First, while our data suggest that Kin17 functions in the splicing of the *flfl* transcript, this will have to be confirmed through further experiments that are able to capture the *flfl* pre-mRNA through sequencing or other methods that will detect the transcript. Second, the presence of redundant mechanisms, such as telophase rescue, may not allow us to see the full effect of the loss of Kin17 in terms of asymmetric cell division and development. While our data suggests that when telophase rescue is also lost, Kin17 does affect cell polarity in telophase indicating Kin17 could potentially lead to defects in cell fate, further studies will have to be carried out to determine the effect this has on development. Thirdly, as we used RNAi, some of the phenotypes may not be fully penetrant, such as Flfl RNAi and PP4-19c RNAi, which may not lead to complete phenotypes and prevent us from determining the full effect on cell polarity that these proteins have.

STAR Methods

Resource availability

Lead contact—Further information and requests for resources and reagents should be directed to and will be fulfilled by the lead contact, Sijun Zhu (zhus@upstate.edu).

Materials availability—All materials generated in this study are available from the lead contact upon request.

Data and code availability

- All data reported in this paper will be shared by the lead contact upon request.
- This paper does not report original code.
- Any additional information required to reanalyze the data reported in this paper is available from the lead contact upon request.

Experimental model and study participant details

Fly Stocks—*insc-Gal4*[6] was used for transgene expression in NBs and *UAS-CD8-GFP*[55] was used to mark neuroblast lineages. UAS transgenes for RNAi knockdown or overexpression include: *UAS-Kin17 RNAi*[60] (#55692; Bloomington Drosophila Stock Center (BDSC) (IN, USA)), *UAS-kin17* (this work), *UAS-kin17-HA* (this work), *UAS-V5-Flfl-PACT* (this work), *UAS-V5-PACT* (this work), *UAS-Mira*^{T591WT}*-GFP* (this work), *UAS-Mira*^{T591D}*-GFP* (this work), *UAS-Mira*^{T591A}*-GFP* (this work), *UAS-RFP-flfl*[21] (#66538, BDSC), *UAS-numb*$^{\Delta CT}$*-GFP*[58], *UAS-flfl RNAi*[21] (#66541, BDSC), *UAS-U2A-RNAi*[56] (#33671; BDSC), *UAS-Sas-4 RNAi*[60] (#35046, BDSC), UAS-EigerIR[61] (#58993; BDSC), and *UAS-PP419c RNAi*[60] (#57823; BDSC). The Mira phosphomimetic alleles, *mira*^{WT}*-HA-mCherry*, *mira*^{S96A}*-HA-mCherry, mira*^{S96D}*-HA-mCherry*24 were generously provided by Jens Januschke. *snRNA:U6atac*$^{k01105\ 62}$ (#10492, BDSC), *flfl*^{n42}[21] (#66534, BDSC), *pros*$^{17\ 63}$ (#5458, BDSC) and *aPKC*$^{K06403\ 62}$ (#10622, BDSC) mutant alleles were used for phenotypic analysis. Mutant chromosomes were balanced over *CyO, weeP* or *TM6B, Tb* for larval analysis and *TM3, Tw-Gal4, UAS-2xGFP* for embryonic analysis. Lines were raised at 25°C on standard fly food. Larva were dissected at 3rd instar larval stage, except for mutants that did not survive until that stage. Embryos were collected at syncytial stages or stages 9–11.

Cell Culture—*Drosophila* S2 cells were grown in Schneider's medium (ThermoFisher Scientific) supplemented with 10% FBS (ThermoFisher Scientific) and 5% streptomycin/penicillin (Gibco) at 37°C.

Method details

RNAi knockdown and transgene analysis—For RNAi knockdown and transgene overexpression, embryos were collected for 24 hours at 25°C, staged at 25°C for an additional 24 hours, and then shifted to 29°C until dissection at third instar larval stages. To visualize RFP-Flfl localization, crosses were collected at 25°C and shifted to 29°C, 24 hrs prior to dissection at third instar larval stages. Crosses involving *UAS-numb*$^{\Delta CT}$*-GFP* were performed at 25°C. For syncytial embryo staining, embryos were collected for 1 hour and staged for 1 hour at 25°C before fixation. For stage 9–11 embryonic NB staining, embryos were collected for 4 hours and staged for 4 hours at 25°C before fixation.

Immunostaining and confocal microscopy—Third instar larval brains were dissected in PBS and fixed within 20 minutes in 4% formaldehyde (Fisher (NH, USA)) in PBS for 20 minutes except for brains stained for Mira which were fixed for 35 minutes. Following fixation and washing, brains were blocked for 30 min in PBS supplemented with 5% normal donkey serum (Jackson Immunoresearch (PA, USA)) and 0.3% Triton X-100 (Fisher). Brains were incubated with primary antibodies overnight at 4°C and secondary antibodies for 2 hours at RT. Embryos were stained as previously described.[64] Coverslips were mounted using antifade reagent in glycerol (Invitrogen). Images were taken using a Zeiss LSM 780 (Zeiss, Germany) inverted confocal microscope using a 40× 1.4 numerical aperture oil immersion objective. Images were collected using Zen Software (Zeiss) and processed with Fiji.[65]

Construction of plasmids and generation of transgenic lines.—For *pUAST-Kin17* and *pUAST-Kin17 HA*, the open reading frame was amplified from a larval brain cDNA library using CloneAmp HiFi PCR Premix (Takara Bio). For the HA-tagged version, the HA tag was integrated into the primer at the c-terminus of Kin17. Primers used were: Kin17 F and Kin17 R or Kin17 HA F and Kin17 HA R. The PCR products were digested by EcoRI and XbaI or XhoI before cloning into the pUAST vector.[59] *UAS-Kin17 and UAS-Kin17 HA* were integrated randomly into the genome of *w1118* embryos and positive lines were mapped. Injections were performed by The Best Gene (Chino Hills, CA, USA).

To generate *pUAST-Mira T591 mutants*, Mira was amplified from genomic DNA using the following primers: Mira F and Mira R. Mira was cloned into pJET using the CloneJet PCR cloning kit (ThermoFisher) and T591A/D mutations were induced using quickchange PCR with the following primers: T591D F and T591D R or T591A F and T591 R. Mira^{WT}, MiraT591A, and Mira^{T591D} were digested from pJET using BglII and XhoI and cloned into pUAST-GFP (see above). *UAS-Mira^{WT}-GFP, UAS-Mira^{T591D}-GFP, and UAS-MiraT591A-GFP* were integrated randomly into the genome of *w^{1118}* embryos and positive lines were mapped. Injections were performed by Rainbow Transgenic Flies, Inc. (CA, USA).

To generate pUAST-V5-PACT and pUAST-V5-Flfl-PACT, Flfl was amplified from a *Drosophila* cDNA library using the Flfl (PACT) F and Flfl (PACT) R primers. The PACT domain of Drosophila Plp was cloned from a cDNA library using the PACT F and PACT R primers. Flfl and PACT were cloned into pUAST-V5 using EcoRI and KpnI. UAS-V5-PACT and UAS-V5-Flfl-PACT were integrated randomly into the genome of *w^{1118}* embryos and positive lines were mapped. Injections were performed by Rainbow Transgenic Flies, Inc. (Camarillo, CA, USA).

Phosphatase assays—S2 cells were lysed in lysis buffer (50 mM Tris-HCl pH 7.4, 50 mM NaCl, 1 mM EDTA, 0.1% NP40) supplemented with HALT protease inhibitor cocktail (Thermo Scientific (MA, USA)). Endogenous PP4 was immunoprecipitated with Protein A/G Plus Agarose beads (Santa Cruz Biotechnology) and 4 μg/mg protein of anti-PP4-19c antibody (Rb, Proteintech (IL, USA)) with anti-IgG (Rb, Invitrogen) as a control. Immunoprecipitation was confirmed by western blotting. The immunoprecipitates were washed three times with TBS and then with Ser/Thr assay buffer (Ser/Thr Phosphatase Assay Kit 1 Millipore Sigma (MA, USA)). We utilized 1 mM phosphoserine peptide generated by (Biomatik, (Canada)) with the sequence, FRTP(pSer)LPQR, corresponding to the S96 region of Mira. The phosphatase assay was carried out using the Ser/Thr Phosphatase Assay Kit 1 following the manufacturer's protocol, with the incubation time of the phosphatase with the peptide increased to 2 hours.

Immunoprecipitation and Immunoblotting—Brains were homogenized in RIPA buffer supplemented with HALT protease inhibitor cocktail and Halt phosphatase inhibitor cocktail (Thermo Scientific). Mira^{WT}-HA-mCherry was precipitated with Protein A/G Plus Agarose beads and 1 μg/mg protein of anti-HA antibody (Rb, Invitrogen). The immunoprecipitates were washed three times with lysis buffer and resuspended in SDS sample buffer.

Lysates/Immunoprecipitates were mixed with SDS sample buffer, separated by SDS-PAGE, transferred to an Immersion-PSQ PVDF membrane (Millipore Sigma), and blotted with indicated primary antibodies. Blots were visualized with SuperSignal West Pico or Femto PLUS Chemoluminescent Substrate (ThermoFisher Scientific) on a BioRad Chemidoc MP Imaging System. For phospho-S96 blots, after probing with the phospho-specific antibody, blots were stripped using mild stripping buffer (1.5% glycine, 0.1% SDS, 1% Tween 20, pH 2.2) and reprobed with HA antibody.

PCR and quantitative real-time PCR—RNA for quantitative Real-time PCR was extracted from 3rd instar larval brains using the Qiagen RNeasy kit, digested with DNase I (NEB) following the manufacturer's protocol, and repurified with the Qiagen RNeasy kit. Primers were designed using Primer3web version 4.1.0 (http://bioinfo.ut.ee/primer3) as recommended by the manufacturer and generated by IDT. Primer used were: eEF1a1 qPCR F, eEF1a1 qPCR R, Flfl qPCR F, and Flfl qPCR R. Optimal concentrations of each primer and primer efficiency were determined, and products were run on an agarose gel to ensure correct products were generated. Real-time PCR reactions were set up using the iTaq Universal SYBR Green One-Step RT-PCR kit (Biorad) according to manufacturer's directions. Reactions were run in triplicate with a BioRad CFX 384 Real Time PCR system. Results were analyzed using the Delta-Delta Ct method. The expression of each transcript was normalized to eEF1a1.[66]

RNA Immunoprecipitation—Embryos expressing Kin17-HA under the control of *insc-Gal4* were collected for 16 hours, dechorionated with 50% bleach, homogenized with a pestle, and lysed in lysis buffer (100 mM KCl, 10 mM Hepes, pH 7.0, 5mM MgCl2, 0.25% Triton, 0.25% NP40, 0.01% SDS, 2x HALT Protease Inhibitor Cocktail (ThermoFisher Scientific), 100 units/ml Ribolock RNase Inhibitor (ThermoFisher Scientific)). One milligram of protein was incubated with 4 µg of antibody (IgG (Rb, Invitrogen) or HA (Rb, Invitrogen)) and 50 µl of Protein A/G Plus agarose beads (Santa Cruz Biotechnology) for 4 hours. Prior to immunoprecipitation, the beads were pre-blocked overnight with single-stranded Salmon Sperm DNA (0.5 mg/ml, Sigma Aldrich). Beads were collected, washed 3 times with wash buffer. RNA was purified using RNAzol RT (Molecular Research Center, Inc. (OH, USA)) following the manufacturer's protocol. RNA was then treated with DNase I (NEB) following the manufacturer's protocol, and 250–500 ng of RNA was used to generate a cDNA library with MMLV H- Reverse transcriptase (Promega) and Random primers (Promega) following the manufacturer's protocol. PCRs were performed using DreamTaq Hot Start Green PCR Master Mix (ThermoFisher Scientific) in 10 µl volume with 1 µl of the RT reaction with the following primers: Flfl RIP F1, Flfl RIP R1, Flfl RIP F2. Flfl RIP R2, aPKC RIP F, aPKC RIP R, Pros RIP F, and Pros RIP R. PCR conditions were as follows: 95°C for 5 min, followed by 30 cycles of 95°C for 30 sec, 54°C for 30 sec, 72°C for 30 sec, and a final extension at 72°C for 5 min. Products were detected on a 1.5% agarose gel by staining with SYBRGold (Invitrogen).

Quantification and statistical analysis

Quantification was performed by pooling neuroblast numbers from multiple brains unless otherwise indicated. Statistical analysis was performed using Microsoft Excel. Pairwise

comparisons were made using two-tailed, paired, or unpaired student's t-tests. Multiple comparisons were performed using two-tailed, paired, or unpaired t-tests with the Bonferroni correction. Data was presented as mean ± standard deviation (SD). P values of <0.05 were considered statistically significant.

To quantify the mitotic index, the ratio of Dpn+, PH3+ NBs to Dpn+ NBs was determined for each brain, with a total of at least 30 NBs counted per brain lobe. The average and standard deviation were calculated from the mitotic index calculated for each brain.

Quantification of nuclear Pros was determined by colocalization of Pros with Deadpan in interphase cells. NBs were determined to be positive for nuclear Pros if the nuclear Pros intensity was greater than 2x than that of the cytoplasmic intensity. The percentage for each brain was determined by quantifying 10 NBs per brain (blinded by turning off the Pros channel during measurement), and the average and standard deviation were calculated from the percentage calculated for each brain. In embryos, quantification was the same except 10 NBs from a single plane were quantified using Mira staining as a guide for nuclear localization (blinded by turning off the Pros channel during measurement).

To quantify colocalization of Mira and Pros at the centrosome in Kin17 RNAi NBs, we first visually identified NBs with a bright spot of Mira staining at the centrosome with the channel of Pros staining turned off, followed by measuring the intensity of Pros and Mira staining at the centrosome and cytoplasm and calculated the ratio. We also did the reverse way by identifying NBs with a bright spot of Pros staining at the centrosome with the channel of Mira staining turned off. The ratio of staining intensity of Pros at the centrosome vs that in the cytoplasm was then plotted against that of Mira or *vice versa*. The significance of correlation was determined by calculating the spearman coefficient (r).

To quantify the Flfl levels in each NB, the average intensity of the Flfl signal for 10 NBs from each brain was quantified and the average intensity for each brain was determined. For each experiment, an average was calculated from the average intensity of each brain and the intensity for the mutants was normalized to that of the control.

Supplementary Material

Refer to Web version on PubMed Central for supplementary material.

Acknowledgments

We thank Drs. J. Januschke, Z. Lipinszki, C. Doe, and Y.N. Jan for antibodies and fly lines; the Bloomington *Drosophila* Stock Center and the TRiP at Harvard Medical School (NIH/NIGMS R01-GM084947) for providing transgenic RNAi fly stocks used in this study; Zhu Lab members for thoughtful discussion and comments; Best Gene, Inc and Rainbow Transgenic Flies Inc for generating transgenic flies, Neuroscience Microscopy Core at Upstate Medical University for providing Zeiss LSM 780 confocal microscopy. This work was supported by the National Institute of Neurological Disorders and Stroke of the National Institutes of Health under Award Number R01NS085232 (S.Z.) and R21NS109748 (S.Z.).

References

1. Gómez-López S, Lerner RG, and Petritsch C (2014). Asymmetric cell division of stem and progenitor cells during homeostasis and cancer. Cellular and Molecular Life Sciences 71, 575–597. 10.1007/s00018-013-1386-1. [PubMed: 23771628]
2. Homem CCF, and Knoblich JA (2012). Drosophila neuroblasts: a model for stem cell biology. Development 139, 4297–4310. 10.1242/dev.080515. [PubMed: 23132240]
3. Hirata J, Nakagoshi H, Nabeshima YI, and Matsuzaki F (1995). Asymmetric segregation of the homeodomain protein Prospero during Drosophila development. Nature 377, 627–630. 10.1038/377627a0. [PubMed: 7566173]
4. Knoblich JA, Jan LY, and Jan YN (1995). Asymmetric segregation of Numb and Prospero during cell division. Nature 377, 624–627. 10.1038/377624a0. [PubMed: 7566172]
5. Bello B, Reichert H, and Hirth F (2006). The brain tumor gene negatively regulates neural progenitor cell proliferation in the larval central brain of Drosophila. Development 133, 2639–2648. 10.1242/dev.02429. [PubMed: 16774999]
6. Betschinger J, Mechtler K, and Knoblich JA (2006). Asymmetric segregation of the tumor suppressor Brat regulates self-renewal in Drosophila neural stem cells. Cell 124, 1241–1253. 10.1016/j.cell.2006.01.038. [PubMed: 16564014]
7. Lee CY, Wilkinson BD, Siegrist SE, Wharton RP, and Doe CQ (2006). Brat is a Miranda cargo protein that promotes neuronal differentiation and inhibits neuroblast self-renewal. Developmental Cell 10, 441–449. 10.1016/j.devcel.2006.01.017. [PubMed: 16549393]
8. Betschinger J, Mechtler K, and Knoblich JA (2003). The Par complex directs asymmetric cell division by phosphorylating the cytoskeletal protein Lgl. Nature 422, 326–330. 10.1038/nature01486. [PubMed: 12629552]
9. Knoblich JA (2010). Asymmetric cell division: recent developments and their implications for tumor biology. Nature reviews. Molecular cell biology 11, 849–860. 10.1038/nrm3010. [PubMed: 21102610]
10. Schuldt AJ, Adams JHJ, Davidson CM, Micklem DR, Haseloff J, St. Johnston D, and Brand AH (1998). Miranda mediates asymmetric protein and RNA localization in the developing nervous system. Genes and Development 12, 1847–1857. 10.1101/gad.12.12.1847. [PubMed: 9637686]
11. Ikeshima-Kataoka H, Skeath JB, Nabeshima YI, Doe CQ, and Matsuzaki F (1997). Miranda directs Prospero to a daughter cell during Drosophila asymmetric divisions. Nature 390, 625–629. 10.1038/37641. [PubMed: 9403694]
12. Shen CP, Jan LY, and Jan YN (1997). Miranda is required for the asymmetric localization of prospero during mitosis in Drosophila. Cell 90, 449–458. 10.1016/S0092-8674(00)80505-X. [PubMed: 9267025]
13. Matsuzaki F, Ohshiro T, Ikeshima-Kataoka H, and Izumi H (1998). Miranda localizes Staufen and Prospero asymmetrically in mitotic neuroblasts and epithelial cells in early *Drosophila* embryogenesis. Development 125, 4089–4098. [PubMed: 9735369]
14. Bailey MJ, and Prehoda KE (2015). Establishment of Par-polarized cortical domains via phosphoregulated membrane motifs. Developmental Cell 35, 199–210. 10.1016/j.devcel.2015.09.016. [PubMed: 26481050]
15. Schober M, Schaefer M, and Knoblich JA (1999). Bazooka recruits inscuteable to orient asymmetric cell divisions in Drosophila neuroblasts. Nature 402, 548–551. 10.1038/990135. [PubMed: 10591217]
16. Wodarz A, Ramrath A, Kuchinke U, and Knust E (1999). Bazooka provides an apical cue for inscuteable localization in Drosophila neuroblasts. Nature 402, 544–547. 10.1038/990128. [PubMed: 10591216]
17. Petronczki M, and Knoblich JA (2001). DmPAR-6 directs epithelial polarity and asymetric cell division of neuroblasts in Drosophila. Nature Cell Biology 3, 43–49. 10.1038/35050550. [PubMed: 11146625]
18. Albertson R, and Doe CQ (2003). Dlg, Scrib and Lgl regulate neuroblast cell size and mitotic spindle asymmetry. Nature Cell Biology 5, 166–170. 10.1038/ncb922. [PubMed: 12545176]

19. Atwood SX, Chabu C, Penkert RR, Doe CQ, and Prehoda KE (2007). Cdc42 acts downstream of Bazooka to regulate neuroblast polarity through Par-6 aPKC. Journal of Cell Science 120, 3200–3206. 10.1242/jcs.014902. [PubMed: 17726059]

20. Atwood SX, and Prehoda KE (2009). aPKC Phosphorylates Miranda to Polarize Fate Determinants during Neuroblast Asymmetric Cell Division. Current Biology 19, 723–729. 10.1016/j.cub.2009.03.056. [PubMed: 19375318]

21. Sousa-Nunes R, Chia W, and Somers WG (2009). Protein Phosphatase 4 mediates localization of the Miranda complex during Drosophila neuroblast asymmetric divisions. Genes and Development 23, 359–372. 10.1101/gad.1723609. [PubMed: 19204120]

22. Zhang F, Huang Z-X, Bao H, Cong F, Wang H, Chai PC, Xi Y, Ge W, Somers WG, Yang Y, et al. (2016). Phosphotyrosyl phosphatase activator facilitates localization of Miranda through dephosphorylation in dividing neuroblasts. Development 143, 35–44. 10.1242/dev.127233. [PubMed: 26586222]

23. Mollinari C, Lange B, and Gonzalez C (2002). Miranda, a protein involved in neuroblast asymmetric division, is associated with embryonic centrosomes of Drosophila melanogaster. Biology of the Cell 94, 1–13. [PubMed: 12000142]

24. Hannaford MR, Ramat A, Loyer N, and Januschke J (2018). aPKC-mediated displacement and actomyosin-mediated retention polarize Miranda in Drosophila neuroblasts. eLife 7, 1–22. 10.7554/eLife.29939.

25. Petritsch C, Tavosanis G, Turck CW, Jan LY, and Jan YN (2003). The Drosophila myosin VI Jaguar is required for basal protein targeting and correct spindle orientation in mitotic neuroblasts. Developmental Cell 4, 273–281. 10.1016/S1534-5807(03)00020-0. [PubMed: 12586070]

26. Angulo JF, Rouer E, Mazin A, Mattei MG, Tissier A, Horellou P, Benarous R, and Devoret R (1991). Identification and expression of the cDNA of KIN17, a zinc-finger gene located on mouse chromosome 2, encoding a new DNA-binding protein. Nucleic Acids Research 19, 5117–5123. 10.1093/nar/19.19.5117. [PubMed: 1923796]

27. Miccoli L, Frouin I, Novac O, Paola DD, Haroer F, Zannis-Hadjopoulos M, Maga G, Biard DSF, and Angulo JF (2005). The human stress-activated protein Kin17 belongs to the multiprotein DNA replication complex and associates in vivo with mammalian replication origins. Molecular and Cellular Biology 25, 3814–3830. 10.1128/MCB.25.9.3814-3830.2005. [PubMed: 15831485]

28. Masson C, Menaa F, Pinon-Lataillade G, Frobert Y, Chevillard S, Radicella JP, Sarasin A, and Angulo JF (2003). Global genome repair is required to activate KIN17, a UVC-responsive gene involved in DNA replication. Proc Natl Acad Sci U S A 100, 616–621. 10.1073/pnas.0236176100. [PubMed: 12525703]

29. Pinon-Lataillade G (2004). KIN17 encodes an RNA-binding protein and is expressed during mouse spermatogenesis. Journal of Cell Science 117, 3691–3702. 10.1242/jcs.01226. [PubMed: 15252136]

30. Zhang Y, Gao H, Gao X, Huang S, Wu K, Yu X, Yuan K, and Zeng T (2017). Elevated expression of Kin17 in cervical cancer and its association with cancer cell proliferation and invasion. International Journal of Gynecological Cancer 27, 628–633. 10.1097/IGC.0000000000000928. [PubMed: 28346239]

31. Zeng T, Gao H, Yu P, He H, Ouyang X, Deng L, and Zhang Y (2011). Upregulation of Kin17 is essential for proliferation of breast cancer. PLoS ONE 6, 1–10. 10.1371/journal.pone.0025343.

32. Huang Q, Zahid KR, Chen J, Pang X, Zhong M, Huang H, Pan W, Yin J, Raza U, Zeng J, et al. (2021). KIN17 promotes tumor metastasis by activating EMT signaling in luminal-A breast cancer. Thoracic Cancer 12, 2013–2023. 10.1111/1759-7714.14004. [PubMed: 34008927]

33. Gao X, Liu Z, Zhong M, Wu K, Zhang Y, Wang H, and Zeng T (2019). Knockdown of DNA/RNA-binding protein Kin17 promotes apoptosis of triple-negative breast cancer cells. Oncology Letters 17, 288–293. [PubMed: 30655766]

34. Ruan L, Jiang W, and Zhang H (2018). Relationships of Kin17 protein expression with clinical features and prognosis of colorectal cancer. Translational Cancer Research 7, 1072–1078. 10.21037/tcr.2018.08.16.

35. Chen J, Xia Y, Peng Y, Wu S, Liu W, Zhang H, Wang T, Yang Z, Zhao S, and Zhao L (2021). Analysis of the association between KIN17 expression and the clinical features/prognosis of

epithelial ovarian cancer, and the effects of KIN17 in SKOV3 cells. Oncology Letters 21, 1–11. 10.3892/ol.2021.12736. [PubMed: 33240407]

36. Zhang Y, Huang S, Gao H, Wu K, Ouyang X, Zhu Z, Yu X, and Zeng T (2017). Upregulation of KIN17 is associated with non-small cell lung cancer invasiveness. Oncology Letters 13, 2274–2280. 10.3892/ol.2017.5707. [PubMed: 28454391]
37. Colonques J, Ceron J, Reichert H, and Tejedor FJ (2011). A transient expression of Prospero promotes cell cycle exit of Drosophila postembryonic neurons through the regulation of Dacapo. PLoS ONE 6, 1–13. 10.1371/journal.pone.0019342.
38. Lai SL, and Doe CQ (2014). Transient nuclear Prospero induces neural progenitor quiescence. eLife 3, 1–12. 10.7554/eLife.03363.
39. Martinez-Campos M, Basto R, Baker J, Kernan M, and Raff JW (2004). The Drosophila pericentrin-like protein is essential for cilia/flagella function, but appears to be dispensible for mitosis. J Cell Biol 165, 673–683. [PubMed: 15184400]
40. Peng CY, Manning L, Albertson R, and Doe CQ (2000). The tumour-suppresor genes lgl and dlg regulate basal protein targeting in Drosophila neuroblasts. Nature 408, 596–600. 10.1038/35046094. [PubMed: 11117748]
41. Wang H, Cai Y, Chia W, and Yang X (2006). Drosophila homologs of mammalian TNF/TNFR-related molecules regulate segregation of Miranda/Prospero in neuroblasts. EMBO Journal 25, 5783–5793. 10.1038/sj.emboj.7601461. [PubMed: 17139248]
42. Lipinszki Z, Lefevre S, Savoian MS, Singleton MR, Glover DM, and Przewloka MR (2015). Centromeric binding and activity of Protein Phosphatase 4. Nature Communications 6, 1–13. 10.1038/ncomms6894.
43. Helps NR, Brewis ND, Lineruth K, Davis T, Kaiser K, and Cohen PTW (1998). Protein phosphatase 4 is an essential enzyme required for organisation of microtubules at centrosomes in *Drosophila* embryos. Journal of Cell Science 111, 1331–1340. 10.1242/jcs.111.10.1331. [PubMed: 9570751]
44. Ou Y, and Rattner JB (2004). The centrosome in higher organisms: structure, composition, and duplication. Int Rev Cytol 238, 119–182. 10.1016/S9974-7696(04)38003-4. [PubMed: 15364198]
45. Gillingham AK, and Munro S (2000). The PACT domain, a conserved centrosomal targeting motif in the coiled-coil proteins AKAP450 and pericentrin. EMBO Reports 1, 524–529. 10.1093/embo-reports/kvd105. [PubMed: 11263498]
46. Januschke J, Llamazares S, Reina J, and Gonzalez C (2011). Drosophila neuroblasts retain the daughter centrosome. Nat Commun 2, 243. 10.1038/ncomms1245. [PubMed: 21407209]
47. Basto R, Lau J, Vinogradova T, Gardiol A, Woods CG, Khodjakov A, and Raff JW (2006). Flies without Centrioles. Cell 125, 1375–1386. 10.1016/j.cell.2006.05.025. [PubMed: 16814722]
48. Mendoza MC, Booth EO, Shaulsky G, and Firtel RA (2007). MEK1 and Protein Phosphatase 4 Coordinate Dictyostelium Development and Chemotaxis. Molecular and Cellular Biology 27, 3817–3827. 10.1128/mcb.02194-06. [PubMed: 17353263]
49. Gaspar VP, Ramos AC, Cloutier P, Pattaro Junior JR, Duarte Junior FF, Bouchard A, Seixas FAV, Coulombe B, and Fernandez MA (2021). Interactome analysis of KIN (Kin17) shows new functions of this protein. Current Issues in Molecular Biology 43, 767–781. 10.3390/cimb43020056. [PubMed: 34449532]
50. Suzuki JMNGL, Osterhoudt K, Cartwright-Acar CH, Gomez DR, Katzman S, and Zahler AM (2022). A genetic screen in C. Elegans reveals roles for KIN17 and PRCC in maintaining 5' splice site identity 10.1371/journal.pgen.1010028.
51. Herold N, Will CL, Wolf E, Kastner B, Urlaub H, Lu R, and Luhrmann R (2009). Conservation of the protein composition and electron microscopy structure of Drosophila melanogaster and human spliceosomal complexes. Molecular and Cellular Biology 29, 281–301. 10.1128/MCB.01415-08. [PubMed: 18981222]
52. Rappsilber J, Ryder U, Lamond AI, and Mann M (2002). Large-scale proteomic analysis of the human spliceosome. Genome Research 13, 1231–1245. 10.1101/gr.473902.
53. Kou WZ, Xu SL, Wang Y, Wang LW, Wang L, Chai XY, and Hua QL (2014). Expression of Kin17 promotes the proliferation of hepatocellular carcinoma cells in vitro and in vivo. Oncology Letters 8, 1190–1194. 10.3892/ol.2014.2244. [PubMed: 25120685]

54. Irion U, Adams J, Chang CW, and St Johnston D (2006). Miranda couples oskar mRNA/Staufen complexes to the bicoid mRNA localization pathway. Developmental Biology 297, 522–533. 10.1016/j.ydbio.2006.05.029. [PubMed: 16905128]
55. Bier E, Vaessin H, Younger-Shepherd S, Jan LY, and Jan YN (1992). deadpan, an essential pan-neural gene in Drosophila, encodes a helix-loop- helix protein similar to the hairy gene product. Genes and Development 6, 2137–2151. 10.1101/gad.6.11.2137. [PubMed: 1427077]
56. Siller KH, Cabernard C, and Doe CQ (2006). The NuMA-related Mud protein binds Pins and regulates spindle orientation in Drosophila neuroblasts. Nature Cell Biology 8, 594–600. 10.1038/ncb1412. [PubMed: 16648843]
57. Wu JS, and Luo L (2006). A protocol for mosaic analysis with a repressible cell marker (MARCM) in Drosophila. Nature Protocols 1, 2583–2589. [PubMed: 17406512]
58. Song Y, and Lu B (2012). Interaction of notch signaling modulator numb with α-adaptin regulates endocytosis of notch pathway components and cell fate determination of neural stem cells. Journal of Biological Chemistry 287, 17716–17728. 10.1074/jbc.M112.360719. [PubMed: 22474327]
59. Brand AH, and Perrimon N (1993). Targeted gene expression as a means of altering cell fates and generating dominant phenotypes. Development 118, 401–415. [PubMed: 8223268]
60. Ni JQ, Liu LP, Binari R, Hardy R, Shim HS, Cavallaro A, Booker M, Pfeiffer BD, Markstein M, Wang H, et al. (2009). A Drosophila resource of transgenic RNAi lines for neurogenetics. Genetics 182, 1089–1100. 10.1534/genetics.109.103630. [PubMed: 19487563]
61. Igaki T, Kanda H, Yamamoto-Goto Y, Kanuka H, Kuranaga E, Aigaki T, and Miura M (2002). Eiger, a TNF superfamily ligand that triggers the Drosophila JNK pathway. EMBO Journal 21, 3009–3018. [PubMed: 12065414]
62. Spradling AC, Stern D, Beaton A, Rhem EJ, Laverty T, Mozden N, Misra S, and Rubin GM (1999). The Berkeley Drosophila Genome Project gene disruption project: Single P-element insertions mutating 25% of vital Drosophila genes. Genetics 153, 135–177. 10.1093/genetics/153.1.135. [PubMed: 10471706]
63. Doe CQ, Chu-LaGraff Q, Wright DM, and Scott MP (1991). The prospero gene specifies cell fates in the Drosophila central nervous system. Cell 65, 451–464. 10.1016/0092-8674(91)90463-9. [PubMed: 1673362]
64. Rothwell WF, and Sullivan W (2000). Fluorescent Analysis of Drosophila Embryos. In Drosophila Protocols., Sullivan W, Ashburner M, Hawley RS, eds. (Cold Spring Harbor Laboratory Press), pp. 141–157.
65. Schindelin J, Arganda-Carrera I, Frise E, Verena K, Mark L, Tobias P, Stephan P, Curtis R, Stephan S, Benjamin S, et al. (2009). Fiji - an Open-Source platform for biological image analysis. Nature Methods 9. 10.1038/nmeth.2019.Fiji.
66. Ponton F, Chapuis MP, Pernice M, Sword GA, and Simpson SJ (2011). Evaluation of potential reference genes for reverse transcription-qPCR studies of physiological responses in Drosophila melanogaster. Journal of Insect Physiology 57, 840–850. 10.1016/j.jinsphys.2011.03.014. [PubMed: 21435341]

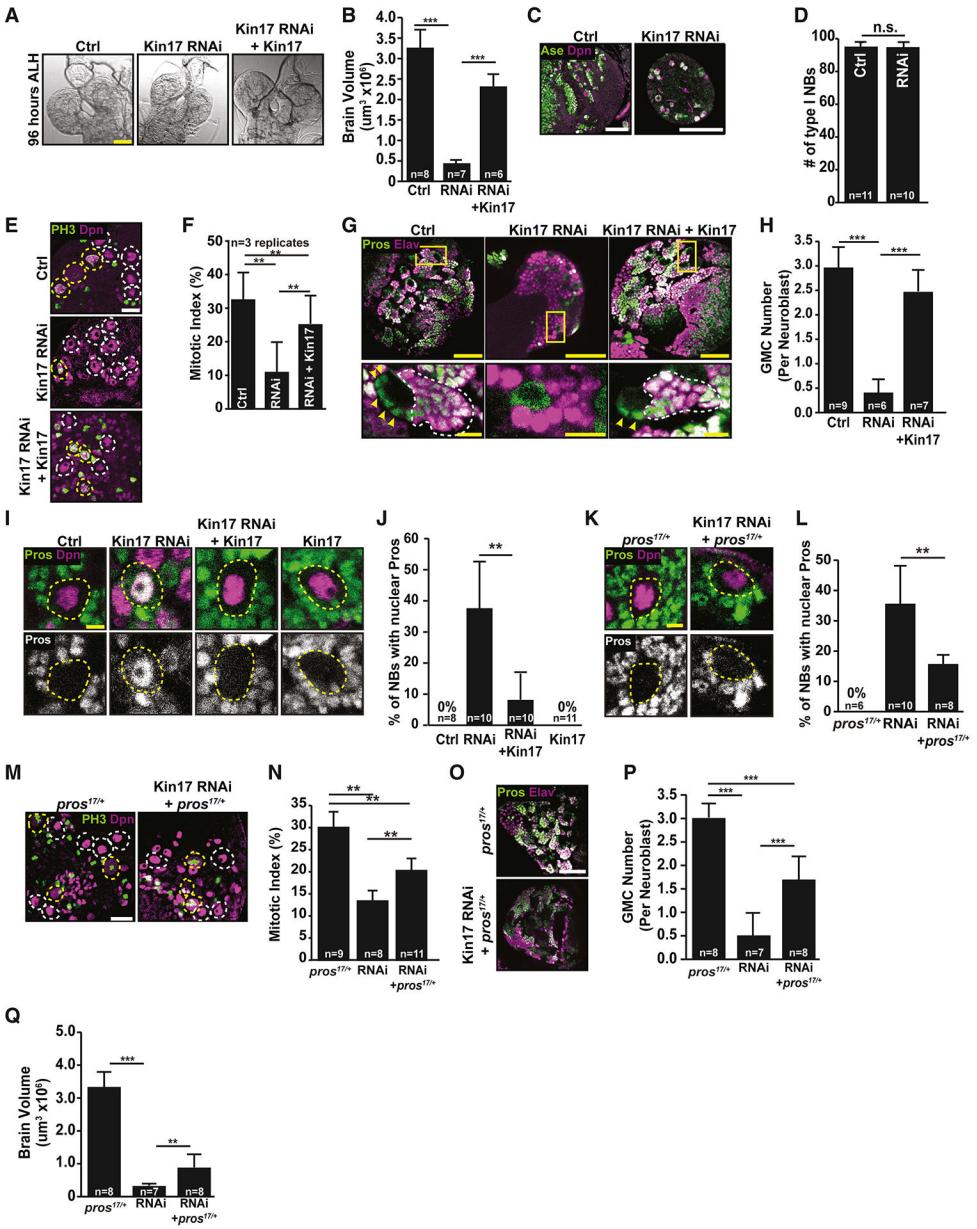

Figure 1. Kin17 knockdown leads to a reduction in brain size and nuclear Pros.

(**A,B**) Brain size in control (ctrl), *Kin17 RNAi*, and Kin17 rescue brains. Scale bar, 50 μm; n ≥ 6 brains. (**C,D**) Quantification of type I neuroblast (NB) number in *Kin17 RNAi* brains. Scale bars, 50 μm; n ≥ 10 brains. (**E,F**) Mitotic index in *Kin17 RNAi*. Yellow circles, mitotic NBs; White circles, non-mitotic NBs; Scale bars, 20 μm; n=3 biological replicates. (**G**) Pros+ progeny in *Kin17 RNAi* brains. Yellow arrowheads, Pros^{+} GMCs; white dashed line, Pros^{+}, Elav^{+} neurons; Scale bars, 50 μm. (**H**) Quantification of GMC number in *Kin17 RNAi* NB lineages. N ≥ 6 brains with each n representing an average of 5 lineages from 1 brain. (**I,J**) Pros staining in *Kin17 RNAi* brains and quantification of the NBs with nuclear Pros. Scale bars, 5 μm; n ≥ 8 brains. (**K,L**) Pros nuclear localization in *Kin17 RNAi; pros$^{17/+}$* NBs. Dashed lines outline NBs. Scale bar, 5 μm; n ≥ 6 brains. (**M,N**) Mitotic index

in *Kin17 RNAi*; *pros*$^{17/+}$ NBs. Yellow circles, mitotic NBs; Grey circles, non-mitotic NBs; Scale bar, 20 μm; n ≥ 8 brains. (**O**) Pros+ progeny in *Kin17 RNAi; pros*$^{17/+}$ brains. Scale bar, 50 μm. (**P**) Quantification of GMC number in *Kin17 RNAi; pros*$^{17/+}$ NB lineages. n ≥ 7 brains with each n represents an average of 5 lineages from 1 brain. (**Q**) Quantification of brain size in *Kin17 RNAi; pros*$^{17/+}$ brains. n ≥ 7 brains. Data are presented as the mean ± 1 Standard deviation (SD). n.s., not significant; **, $p<0.01$; ***, $p<0.001$, unpaired student's t-test for (D) and unpaired student's t-test with the Bonferroni correction for (B, H, J, L, N, P, Q).

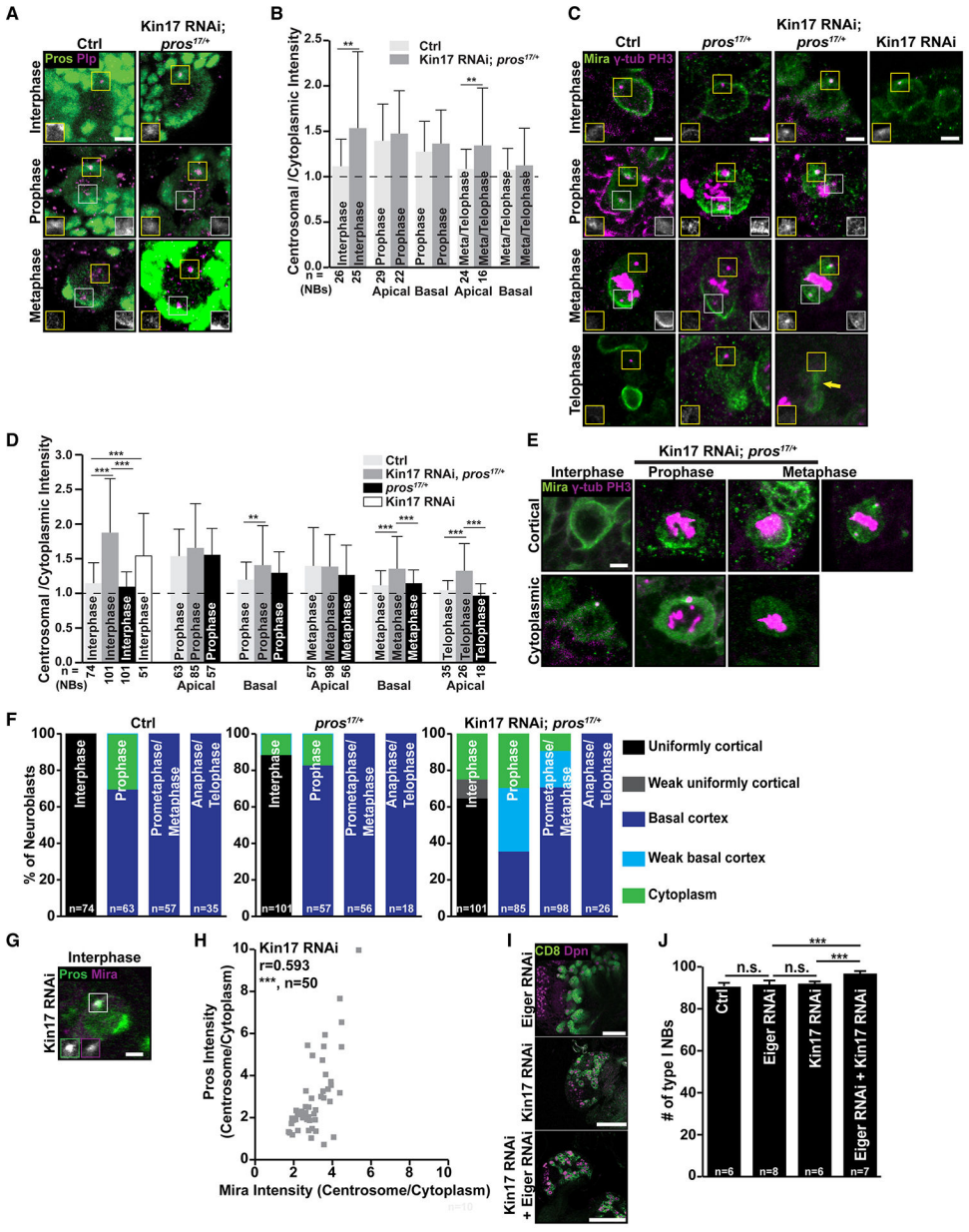

Figure 2. Kin17 knockdown leads to centrosomal localization of Pros and Mira.

(**A,B**) Pros localization to the centrosome (marked by Pericentrin-like protein (Plp)) in ctrl and *Kin17 RNAi*; *pros*$^{17/+}$ NBs. Inset, Pros localization at apical (yellow boxes) and basal (grey boxes) centrosomes; Scale bars, 5 μm; n ≥ 16 NBs. (**C,D**) Mira localization in ctrl, Kin17 RNAi, *pros*$^{17/+}$, and *Kin17 RNAi pros*$^{17/+}$ NBs throughout the cell cycle. Inset, Mira localization at apical (yellow boxes) and basal (grey boxes) centrosomes; Arrow, Mira localization on spindle; Scale bar, 5 μm; n ≥ 18 NBs. (**E,F**) Cortical localization of Mira in ctrl, *pros*$^{17/+}$, and *Kin17 RNAi pros*$^{17/+}$ NBs. Metaphase depicts normal (left) and weak (right) basal cortical localization of Mira. Scale bars, 5 μm; n ≥ 18 NBs. (**G,H**) Colocalization of Mira and Pros at the centrosome in *Kin17 RNAi* NBs. Insets, Grey boxes, Pros; Purple boxes, Mira; Scale bar, 5 μm; r, Spearman coefficient; n = 50 NBs. (**I,J**)

Neuroblast numbers in Kin17 and Eiger single knockdown or double knockdown brains. Scale bar, 5 μm; n ≥ 6 brains. Data are presented as the mean ± 1 SD. n.s., not significant; **, $p<0.001$; ***, $p<0.001$, unpaired student's t-test for (B), unpaired student's t-test with the Bonferroni correction for (D, J), and Spearmann's rank correlation coefficient for (H). See also Figures S1 and S2.

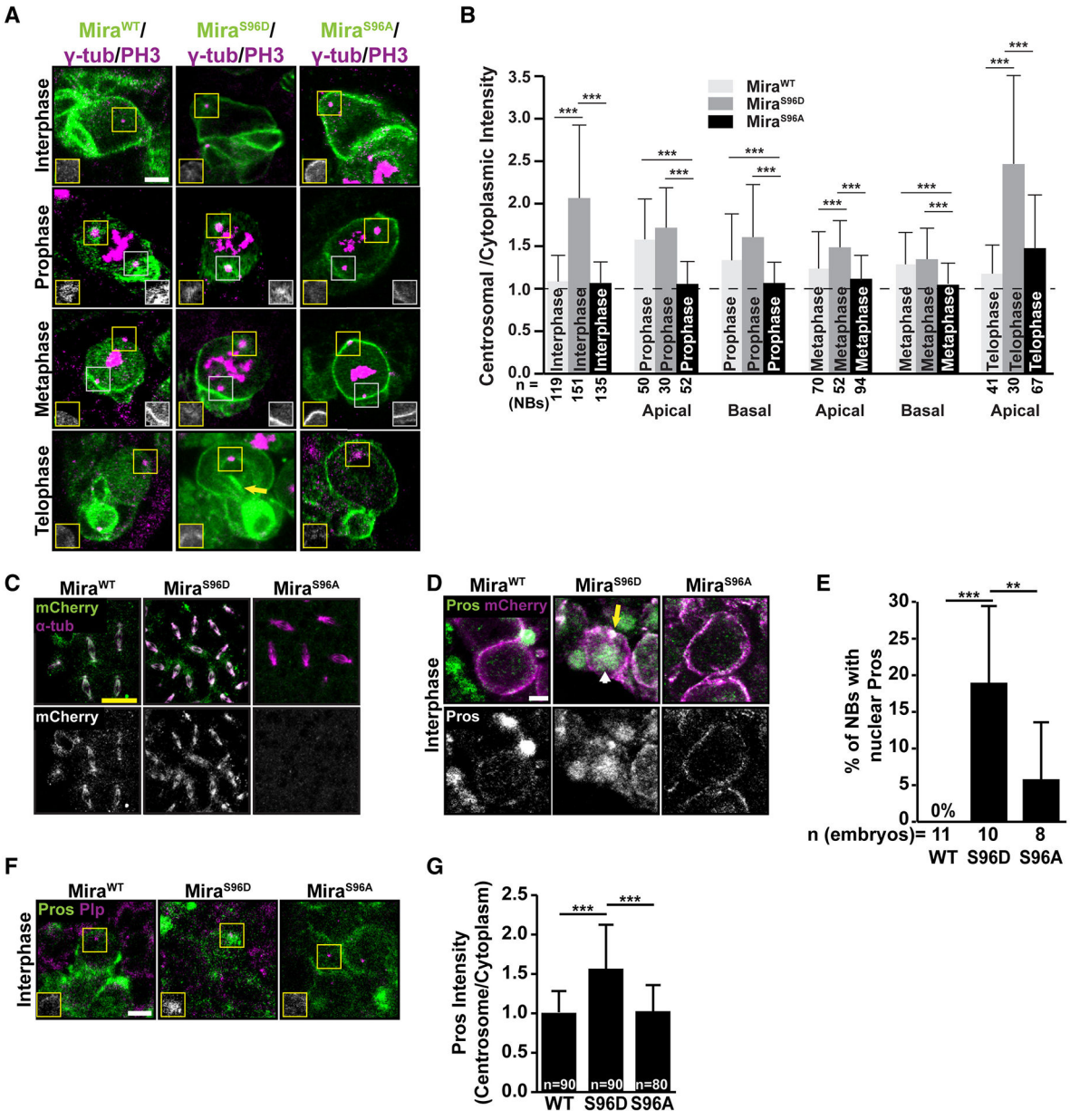

Figure 3. Phosphorylation of Mira residue S96 is required and sufficient for centrosomal localization.

(**A,B**) Localization of Mira^{WT}-mCherry, Mira^{S96D}-mCherry, and Mira^{S96A}-mCherry in NBs. Inset, Mira localization at apical (yellow boxes) and basal (grey boxes) centrosomes; Arrow, spindle localization of Mira; Scale bar, 5 μm; n ≥ 30 NBs. (**C**) Localization of Mira^{WT}-mCherry, Mira^{S96D}-mCherry, and Mira^{S96A}-mCherry in syncytial embryos. Scale bar, 25 μm. (**D,E**) Nuclear localization of Pros in embryonic NBs homozygous for Mira^{WT}-mCherry, Mira^{S96D}-mCherry, and MiraS96A-mCherry. Arrow, centrosome; Arrowhead, nuclear Pros; Scale bar, 5 μm; n ≥ 8 embryos. (**F,G**) Pros localization to the centrosome in interphase embryonic NBs homozygous for Mira^{WT}-mCherry, Mira^{S96D}-mCherry, and MiraS96A-mCherry. Yellow boxes, Pros localization at the centrosome; Scale bar, 5 μm;

n ≥ 80 NBs. Data are presented as the mean ± 1 SD. **, $p<0.01$; ***, $p<0.001$, unpaired student's t-test with the Bonferroni correction. See also Figure S3.

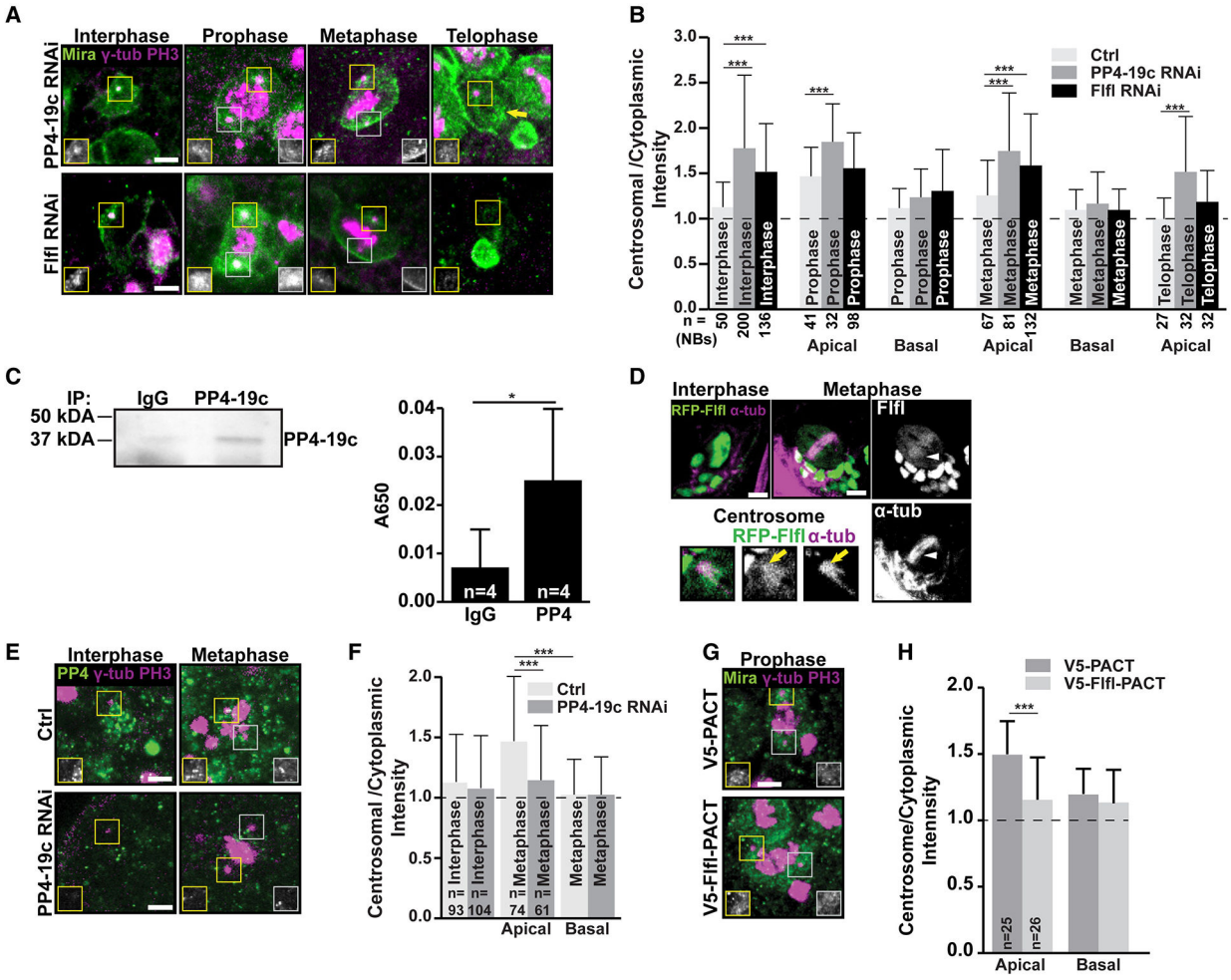

Figure 4. PP4 is required for displacement of Mira from the centrosome.

(**A,B**) Localization of Mira in *PP4-19c* and *Flfl RNAi* NBs throughout the cell cycle. Inset, Mira localization at apical (yellow) and basal (grey) centrosomes; Scale bar, 5 μm; n ≥ 27 NBs. (**C**) IP of PP4-19c (left) and quantification of dephosphorylation of Mira phosho-Serine96 peptide by PP4 precipitates (right). n = 4 biological replicates. (**D**) Localization of RFP-Flfl in NBs. Arrowheads, mitotic spindle; Arrows, centrosome; Scale bar, 5 μm. (**E,F**) Localization of PP4-19c in ctrl and *PP4-19c RNAi* NBs. Inset, PP4-19c localization at apical (yellow) and basal (grey) centrosomes; Scale bar, 5 μm; n ≥ 61 NBs. (**G,H**) Localization of Mira in prophase NBs expressing V5-PACT or V5-Flfl-PACT. Inset, Mira localization at apical (yellow boxes) and basal (grey boxes) centrosomes; Scale bar, 5 μm; n ≥ 25 NBs. Data are presented as the mean ± 1 SD. n.s., not significant; *, $p<0.05$; **, $p<0.01$; ***, $p<0.001$, paired student's t-test for (C), unpaired student's t-test for (H), and unpaired Student's t-test with the Bonferroni correction for (B, F). See also Figure S4.

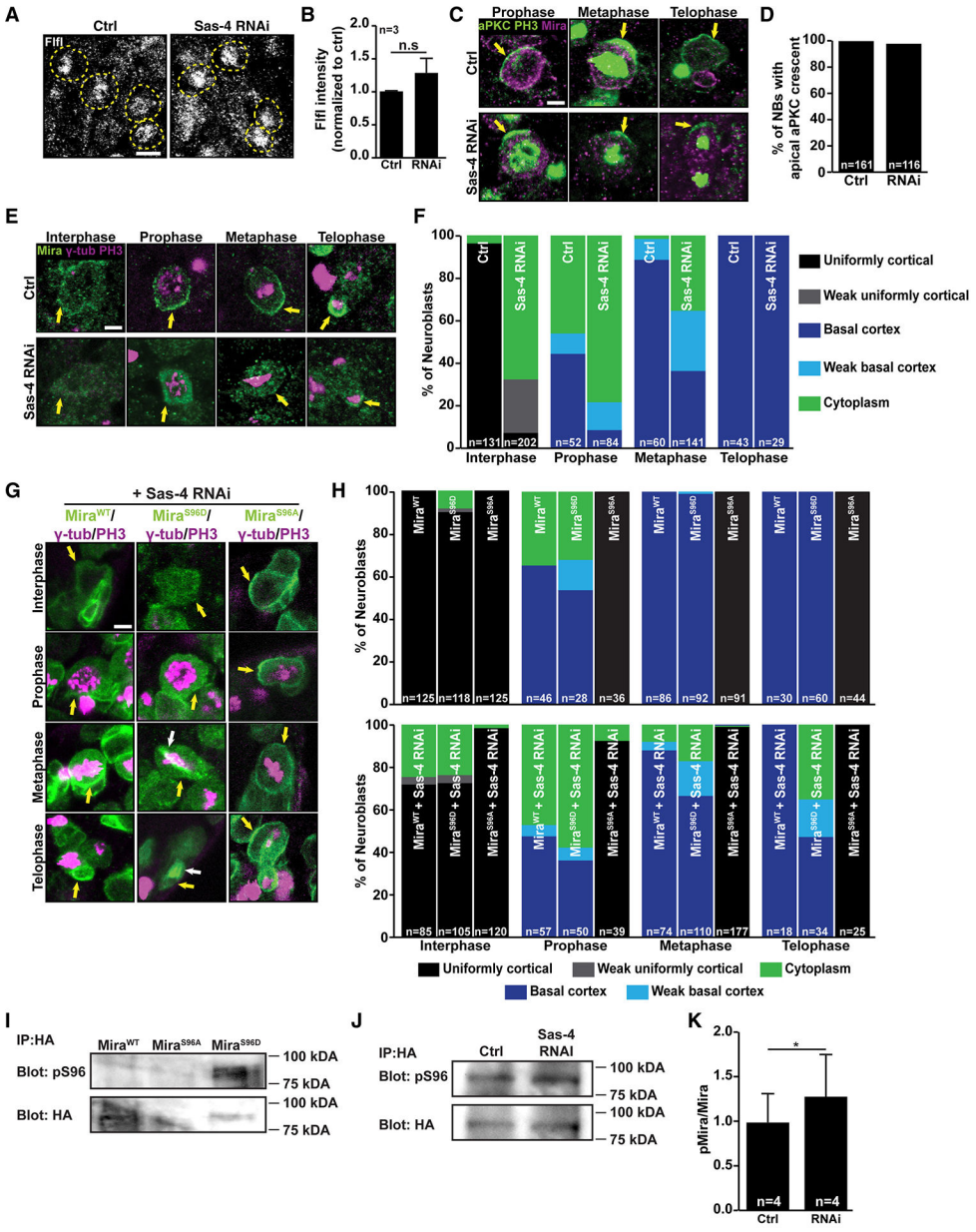

Figure 5. Centrosomes are required for proper localization and dephosphorylation of Mira.

(**A,B**) Flfl levels in *Sas-4 RNAi* NBs. Dotted lines, NBs; Scale bar, 10 μm; n = 3 biological replicates. (**C,D**) aPKC localization in *Sas-4 RNAi* NBs. Arrows, apical aPKC crescent; Scale bar, 5 μm; n ≥ 116 NBs. (**E,F**) Cortical localization of Mira in *Sas-4* RNAi NBs. Yellow arrows, cortex; Scale bar, 5 μm; n ≥ 29 NBs. (**G,H**) Localization of Mira in NBs expressing *Sas-4 RNAi* in combination with Mira^{WT}, Mira^{S96D}, and MiraS96A. Yellow arrows, cortex; white arrows, mitotic spindle; Scale bar, 5 μm; n ≥ 25 NBs. (**I**) Verification of specificity of antibody to recognize phosphorylated S96 of Mira. (**J,K**) Levels of phosphorylated S96 in ctrl and *Sas-4* RNAi brains. n = 4 biological replicates. Data are presented as the mean ± 1 SD. n.s., not significant; *, $p<0.05$, paired student's t-test for (B, K) and unpaired student's t-test for (D).

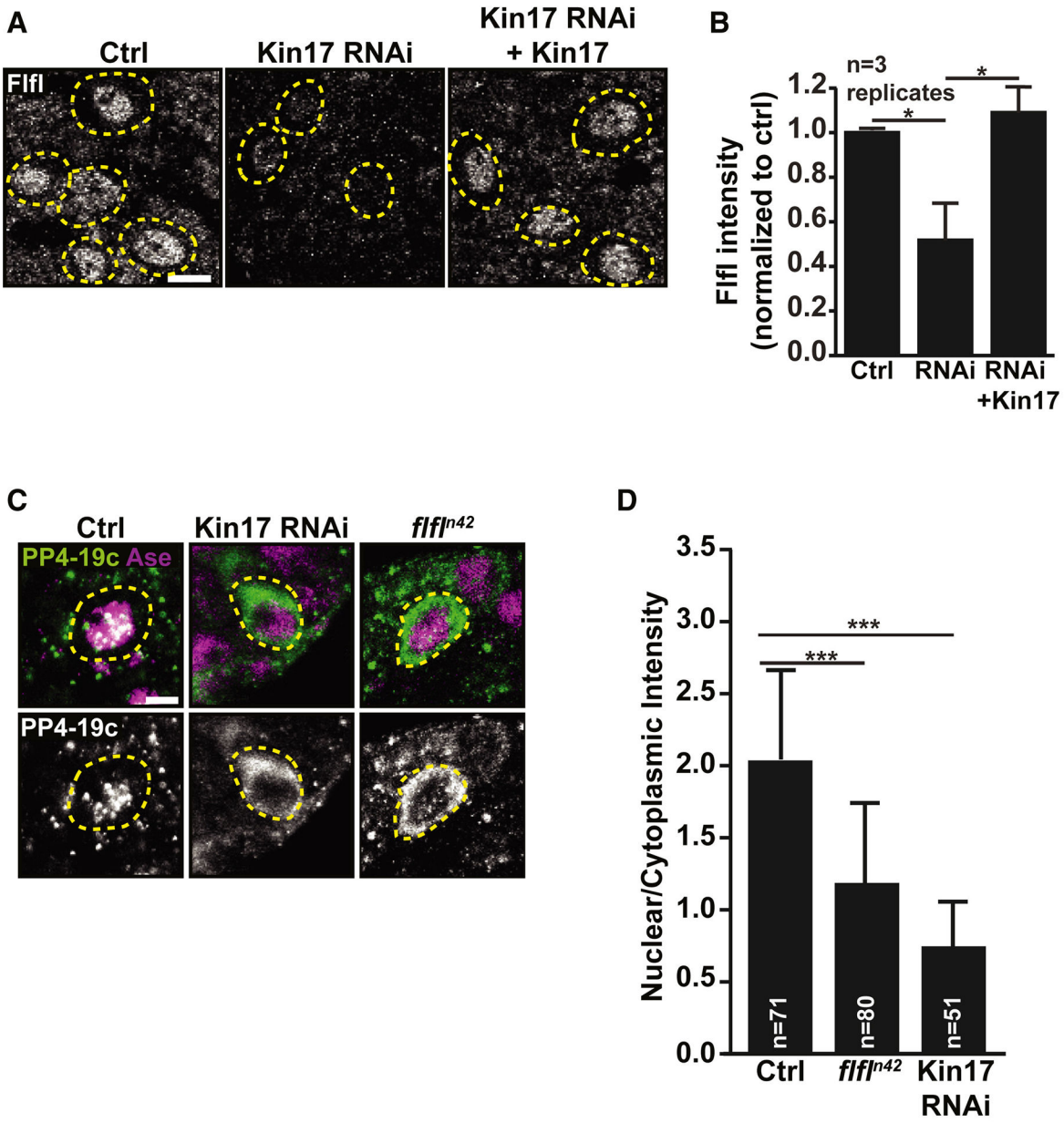

Figure 6. Kin17 regulates Flfl levels and functions upstream of Flfl.

(**A,B**) Relative Flfl levels in ctrl, *Kin17 RNAi*, and Kin17 rescue NBs. Dotted lines, NBs [identified by size and CD8-GFP expression (not shown)]; Scale bar, 5 μm; n = 3 biological replicates. (**C,D**) PP4-19c localization in *Kin17 RNAi* and *flfl*^{n42} NBs. Dashed circles, NBs. Ase staining indicates nucleus. Scale bar, 5 μm; n ≥ 51 NBs. Data are presented as the mean ± 1 SD. *, $p<0.05$; ***, $p<0.001$, paired student's t-test with the Bonferroni correction for (B) and unpaired student's t-test with the Bonferroni correction for (D).

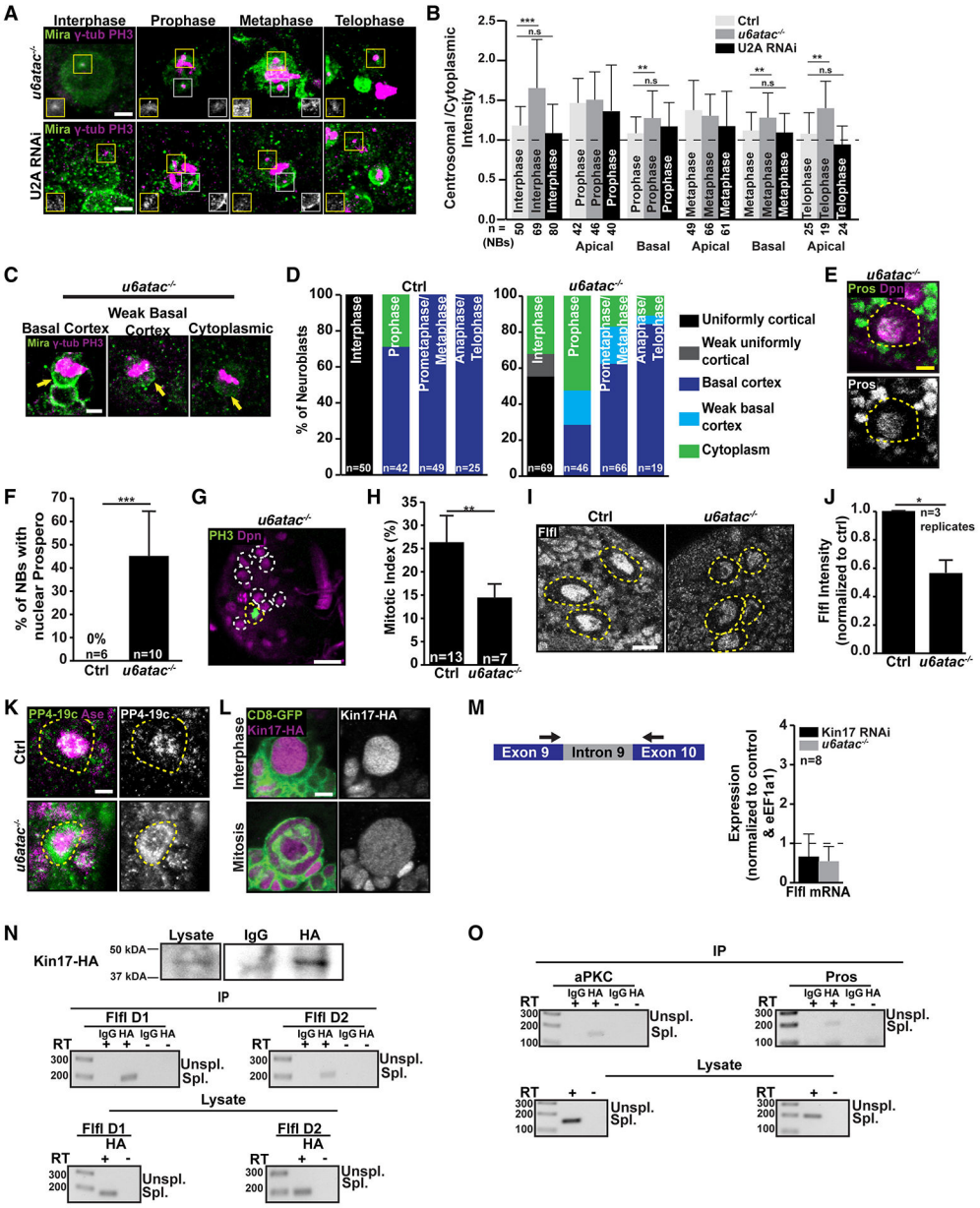

Figure 7. Kin17 regulates splicing of the *flfl* pre-mRNA.

(**A,B**) Localization of Mira throughout the cell cycle in *u6atac*^{K01105} (*u6atac*$^{-/-}$) mutant and U2A RNAi NBs. Inset, Mira localization at apical (yellow boxes) and basal (grey boxes) centrosomes; Scale bar, 5 μm; n ≥ 19 NBs. (**C,D**) Cortical localization of Mira in metaphase *u6atac*$^{-/-}$ NBs. Arrows, basal cortex. Scale bar, 5 μm; n ≥ 19 NBs. (**E,F**) Pros nuclear localization in *u6atac*$^{-/-}$mutant NBs. Dashed circles outline NBs. Scale bar, 5 μm; n ≥ 6 brains. (**G,H**) Mitotic Index in *u6atac*$^{-/-}$ mutant brains. Yellow circles, mitotic NBs; Grey circles, non-mitotic NBs; Scale bar, 20 μm; n ≥ 7 brains. (**I,J**) Flfl staining in *u6atac*$^{-/-}$ mutant NBs. Dashed circles, NBs; Scale bar, 10 μm; n = 3 biological replicates. (**K**) PP4-19c staining in *u6atac*$^{-/-}$ mutant NBs. Dashed circles, NBs; Scale bar. (**L**) Localization of Kin17-HA in NBs during interphase and mitosis. Scale bar, 5 μm. (**M**) Quantitative

RT-PCR results for Flfl transcript. Left panel, position of primers. n = 8 biological replicates (**N**) RNA immunoprecipitation of *flfl* mRNA by Kin17-HA in *Drosophila* embryos. Top panel, IP of Kin17-HA proteins; Bottom panels, *flfl* RT-PCR products obtained from cDNA libraries generated from RIP immunoprecipitates. Lysate and IP samples were run on the same blot but images were taken from different exposures. (**O**) aPKC and Pros RT-PCR results obtained from cDNA libraries generated from RIP immunoprecipitates. Data are presented as the mean ± 1 SD. n.s., not significant; *, $p<0.05$; **, $p<0.01$; ***, $p<0.001$, unpaired student's t-test with Bonferroni correction (B). unpaired Student's t-test for (F, H), and paired Student's t-test for (J).

Key resources table

REAGENT or RESOURCE	SOURCE	IDENTIFIER
Antibodies		
Rabbit polyclonal PP4-19c (IP: 4 μg/mg; IF: 1:1000; IB: 1:1000)	Proteintech	#10262-1-AP
Rabbit monoclonal HA (IP: 1μg/mg; IF: 1:500; IB: 1:1000)	Invitrogen	#3724
Guinea Pig Ase (IF: 1:5000)	Y.N. Jan	N/A
Rabbit Dpn (IF: 1:500)	Y.N. Jan[1]	N/A
Mouse monoclonal Pros (IF: 1:5 (cortical/centrosomal), 1:50 (nuclear))	Developmental Hybridoma Studies Bank	**#Prospero (MR1A)**
Rabbit polyclonal Plp (IF: 1:500)	Abcam	#4448
Mouse monoclonal PH3 (IF: 1:1000)	Cell Signaling Technology	#9706
Mouse monoclonal Elav (IF: 1:100)	Developmental Hybridoma Studies Bank	**#Elav-9F8A9**
Mouse monoclonal α-tub (IF: 1:1000)	Sigma	#T199
Mouse monocolonal γ-tub (IF: 1:1000)	Sigma	#T5326
Rabbit Mira (IF: 1:1000)	Y.N. Jan	N/A
Rat Flfl (IF: 1:500)	Z. Lipinszki[2]	N/A
Guinea Pig Baz (IF: 1:500)	C. Doe[3]	N/A
Mouse monoclonal aPKC (IF: 1:500)	Santa Cruz Biotechnology	**#sc-17781**
Chicken polyclonal GFP (IF: 1:500)	Aves Lab	#GFP-1010
Rabbit DsRed (IF: 1:500)	Takara Bio	#632496
Chicken Alexafluor-488 (IF: 1:500)	Invitrogen	#A-11039
Rabbit Alexafluor-647 (IF: 1:500)	Invitrogen	#A-21245
Mouse Alexafluor-647 (IF: 1:500)	Invitrogen	#A-21235
Rabbit Rhodamine Red RRX (IF: 1:500)	Jackson Immunoresearch	#611-295-215
Rat Rhodamine Red RRX (IF: 1:500)	Jackson Immunoresearch	#712-295-153
Mouse Rhodamine Red RRX (IF: 1:500)	Jackson Immunoresearch	#712-295-150
Rabbit IgG (IP: 1–4 μg/mg)	Invitrogen	#02–6102
Rabbit polyclonal Phospho-(Ser) 14-3-3 binding motif (IB: 1:1000)	Cell Signaling Technology	#9601S
Rabbit HRP (IB: 1:2000)	Cell Signaling Technology	#7074
Rabbit HRP (IB 1:2000)	Jackson Immunoresearch	#112-035-003
Bacterial and virus strains		
DH5 alpha E. coli		
Biological samples		
Chemicals, peptides, and recombinant proteins		
Normal Donkey Serum	Jackson Immunoresearch	#017-000-121

REAGENT or RESOURCE	SOURCE	IDENTIFIER
Triton X-100	Fisher	#AAA16046AE
37% Formaldehyde	Fisher	#F79-1
HALT protease inhibitor cocktail	Thermo Scientific	#78430
HALT Phosphatase inhibitor cocktail	Thermo Scientific	#78420
Fetal Bovine Serum	Thermo Scientific	#26150079
Penicillin/Streptomycin	Thermo Scientific	#15140122
FRTP(pSer)LPQR	Biomatik	N/A
Critical commercial assays		
Ser/Thr Phosphatase Assay Kit 1	Millipore Sigma	#17-127
iTaq Universal Sybr Green One-Step RT PCR kit	Biorad	#1725120
Deposited data		
Experimental models: Cell lines		
D. melanogaster S2 cells	F. Pignoni	N/A
Experimental models: Organisms/strains		
D. melanogaster insc-Gal4	J. Knoblich[4]	N/A
D. melanogaster UAS-CD8-GFP	L. Luo[5]	N/A
D. melanogaster UAS-Kin17 RNAi (y^1, sc, v^1, sev^{21}; P{TRIP.HMC03906}attP40)*	Bloomington Drosophila Stock Center	#55692; http://flybase.org/reports/FBal0294464
D. melanogaster UAS-Kin17	This work	N/A
D. melanogaster UAS-Kin17-HA	This work	N/A
D. melanogaster UAS-V5-flfl-PACT	This work	N/A
D. melanogaster UAS-V5-PACT	This work	N/A
D. melanogaster UAS-$Mira^{T591WT}$-GFP	This work	N/A
D. melanogaster UAS-$Mira^{T591D}$-GFP	This work	N/A
D. melanogaster UAS-$Mira^{T591A}$-GFP	This work	N/A
D. melanogaster UAS-RFP-Flfl	Bloomington Drosophila Stock Center	#66538; http://flybase.org/reports/FBal0322866
D. melanogaster UAS-Flfl RNAi	Bloomington Drosophila Stock Center	#66541; http://flybase.org/reports/FBal0322868
D. melanogaster UAS-$numb^{\Delta CT}$-GFP	B. Lu[6]	http://flybase.org/reports/FBtp0073064
D. melanogaster UAS-U2A RNAi (y^1, sc, v^1, sev^{21}; P{TRIP.HMS00535}attP2/TM3, Sb^1)*	Bloomington Drosophila Stock Center	#33671; http://flybase.org/reports/FBal0257223
D. melanogaster UAS-Sas4 RNAi (y^1, sc, v^1, sev^{21}; P{TRIP.HMS01463}attP2)*	Bloomington Drosophila Stock Center	#35049; http://flybase.org/reports/FBal0263371

REAGENT or RESOURCE	SOURCE	IDENTIFIER
D. melanogaster UAS-EigerIR	Bloomington Drosophila Stock Center	#58993; http://flybase.org/reports/FBti0164915
D. melanogaster UAS-PP4-19c RNAi (y^1, v^1; P{TRIP.HMJ21831}attP40)	Bloomington Drosophila Stock Center	#57823; http://flybase.org/reports/FBal0300358
D. melanogaster $mira^{WT}$-HA-mcherry	J. Januschke[7]	http://flybase.org/reports/FBal0361098
D. melanogaster $mira^{S96D}$-HA-mcherry	J. Januschke[7]	http://flybase.org/reports/FBal0361230
D. melanogaster $mira^{S96A}$-HA-mcherry	J. Januschke[7]	http://flybase.org/reports/FBal0361228
D. melanogaster snRNA:U6atac ^{k01105}	Bloomington Drosophila Stock Center	#10492; http://flybase.org/reports/FBal0064601
D. melanogaster flfl ^{n42}	Bloomington Drosophila Stock Center	#66534; http://flybase.org/reports/FBal0241927
D. melanogaster pros ^{17}	Bloomington Drosophila Stock Center	#5458; http://flybase.org/reports/FBal0032479
D. melanogaster aPKC ^{k06403}	Bloomington Drosophila Stock Center	#10622; http://flybase.org/reports/FBal0064438
Oligonucleotides		
Random primers	Invitrogen	#481900111
Kin17 F: 5'GGAATTCATGGGTCGCGCCGAGGTA-3'	This work, IDT	N/A
Kin17 R: 5'-GCTCTAGACTAGGCGCCATGTAGTTTAGATAT-3'	This work, IDT	N/A
Kin17 HA F: 5'-ATCGATGAATTCATGGGTCGCGCCGAGGTAGGT-3'	This work, IDT	N/A
Kin17 HA R: 5'-ATCGATCTCGAGTTCCTAAGCGTAATCTGGAACATCGTAAGGGTAGGCGCCATGTAGTTTAGATAT-3'	This work, IDT	N/A
Mira F: 5'-TTCAGTAGATCTATGTCTTTCTCCAAGGCCAAG-3'	This work, IDT	N/A
Mira R: 5'-TTCAGTCTCGAGGATGTTGCGCGCCTTGAGCAC-3'	This work, IDT	N/A
T591D F: 5'-CTGAGATCCTCCTCCCAGGATCTGCAGAGCGAGGTATCG-3'	This work, IDT	N/A
T591D R: 5'-CGATACCTCGCTCTGCAGATCCTGGGAGGAGGATCTCAG-3'	This work, IDT	N/A
T591A F: 5'-CTGAGATCCTCCTCCCAGGCCCTGCAGAGCGAGGTATCG-3'),	This work, IDT	N/A
T591A R: 5'-CGATACCTCGCTCTGCAGGGCCTGGGAGGAGGATCTCAG-3'	This work, IDT	N/A
Flfl (PACT) F: 5'- GAATTCATGACGACTGACACCCGCCGAC-3'	This work, IDT	N/A
Flfl (PACT) R: 5'-GAATTCTGCCTGACGCGCGCGCTTTTGTGC-3'	This work, IDT	N/A
PACT F: 5'- GGTACCTTATTGCTCTGCAGAAGAAATGCG-3'	This work, IDT	N/A
PACT R: 5'- GGTACCATGATGCCGCGCATGCGCTC-3'	This work, IDT	N/A
eEF1a1 qPCR F: 5'-CTACAAGTGCGGTGGTATCG	This work, IDT	N/A
eEF1a1 qPCR R: 5'-TTATCCAAAACCCAGGCGTA-3'	This work, IDT	N/A
Flfl qPCR F: 5'-CTCCAGCTGTGTCCAGTCC-3'	This work, IDT	N/A

REAGENT or RESOURCE	SOURCE	IDENTIFIER
Flfl qPCR R: 5'-TCGTAGTCATCTTCGCCAGA-3'	This work, IDT	N/A
Flfl RIP F1: 5'-CCACGTGTCATCCACCTATG-3'	This work, IDT	N/A
Flfl RIP R1: 5'-CTCAGGGCCAGATCAAAGTTAT-3'	This work, IDT	N/A
FlflI RIP F2: 5'-TAGAGTTCTCGCCTCTGGTAG-3'	This work, IDT	N/A
FlflI RIP R2: 5'-CCTTCTCGGTGAGCATGTTT-3'	This work, IDT	N/A
aPKC RIP F: 5'-CAGCATCTATCGACGCGGTGC-3'	This work, IDT	N/A
aPKC RIP R: 5'-CTGACGTCCCAAACCCCAGAT-3'	This work, IDT	N/A
Pros RIP F: 5'-GCACGACAAGCTGTCACCGA-3'	This work, IDT	N/A
Pros RIP R: 5'-CTCGTGTCTTTGCCACCCT-3'	This work, IDT	N/A
Recombinant DNA		
pUAST vector	N. Perrimon[8]	N/A
Software and algorithms		
ImageJ (Fiji)	http://fiji.sc	N/A
Zen software	Zeiss	N/A
Other		
Antifade Reagent in Glycerol	Invitrogen	#S36936
Zeiss LSM 780 inverted confocal microscope	Zeiss	N/A
Protein A/G Plus Agarose Beads	Santa Cruz Biotechnology	#sc-2003
Immersion-P^{SQ} PVDF membrane	Millipore Sigma	#ISEQ00010
SuperSignal West Pico PLUS Chemoluminescent Substrate	ThermoFisher Scientific	#34579
SuperSignal West Femto Chemiluminescent Substrate	ThermoFisher Scientific	#34094
CloneAmp HiFi PCR Premix	Takara Bio	#639298
Schneiders Medium	ThermoFisher Scientific	#21720024
RNeasy Kit	Qiagen	#74104
RNAzol RT	Molecular Research Center Inc	#RN 190
Ribolock RNase Inhibitor	ThermoFisher Scientific	#EO0381
Salmon Sperm DNA	Sigma Aldrich	#7656
Proteinase K	Sigma Aldrich	#124568
DNase I	New England Biolabs	#M0303
MMLV H- Reverse transcriptase	Promega	#M5301
DreamTaq Hot Start Green PCR Master Mix	ThermoFisher Scientific	#K9021
EcoRI	ThermoFisher Scientific	#ER0271
XhoI	ThermoFisher Scientific	#ER0692
XbaI	ThermoFisher Scientific	#ER0682
BglII	ThermoFisher Scientific	#ER0082

REAGENT or RESOURCE	SOURCE	IDENTIFIER
KpnI	ThermoFisher Scientific	#ER0521
CloneJet PCR Cloning Kit	ThermoFisher Scientific	#K1231
SYBR Gold	Invitrogen	#S11494